UNIVERSITY OF ROCHESTER

DOCTORAL THESIS

Neural Tuning in High-Dimensional Stimulus Spaces

Author:
Hayden SCOTT

Supervisor:
Adam SNYDER

Submitted in partial fulfillment of the requirements
for the degree of Doctor of Philosophy

in the Department of

Brain and Cognitive Sciences
School of Arts and Sciences
University of Rochester
Rochester, NY

July 1, 2022

Contents

Biographical Sketch

The author was born in Louisville, KY, USA. He attended The University of Kentucky and graduated with a Bachelor of Science in Neuroscience. He received a Masters degree in Brain and Cognitive Sciences from the University of Rochester in 2020. He began doctoral studies in Brain and Cognitive Sciences at the University of Rochester in 2020. He was awarded nothing Fellowship in never and always[if applicable (it's not)].

He was awarded a Name(s) Fellowship in 200X and 200X][if applicable]. He pursued his research in neural computations underlying feature based attention under the direction of Dr. Adam Snyder.

The following publications were a result of work conducted during doctoral study: [list full bibliographic reference information in the format used elsewhere in the dissertation] Publication A Publication B Etc.

Acknowledgements

The acknowledgments and the people to thank go here, don't forget to include your project advisor...

Adam Snyder

Ellie Sachse

Megan Conley

Chad Dekdebrun

Rolo Wrapper

Gremlin Mononym

UNIVERSITY OF ROCHESTER

Abstract

Faculty Name

Brain and Cognitive Sciences

Doctor of Philosophy

Neural Tuning in High-Dimensional Stimulus Spaces

by Hayden SCOTT

The Thesis Abstract is written here (and usually kept to just this page). The page is kept centered vertically so can expand into the blank space above the title too…

List of Tables

List of Figures

List of Symbols

a	distance	m
P	power	W ($\mathrm{J\,s^{-1}}$)
ω	angular frequency	rad
θ	orientation	deg°

List of Abbreviations

GAN	**G**enerative **A**dversarial **N**etwork
CNN	**C**onvolutional **N**eural **N**etwork
MI	**M**utual **I**nformation
HF	Entropy (**H**) **F**actor
RGC	**R**etinal **G**anglion **C**ells
LGN	**L**ateral **G**eniculate **N**ucleus
IT	**I**nferior **T**emporal cortex
MT	**M**iddle **T**emporal area

Chapter 1

Introduction

Humans are incredibly visual animals. We rely on our sight to effectively navigate the world around us, which has lead to extensive research over the last few decades into the machinations of our brain that allow this. Most laymen would agree that light enters our eyes and this information is then processed by the brain, but the specific computations that occur have only begun to be elucidated with recent developments in artificial neural networks. These evolving methods for describing neural computations parallels more sophisticated electrophysiological techniques, such as high-yield neural recordings capable of recording hundreds-to-thousands of neurons simultaneously. This intersection of artificial and biological intelligence has brought about as many problems as it has solutions, including the curse of dimensionality, noise, and the black-box problem. I will focus first on a brief history of visual neuroscience, and introduce the idea of stimulus tuning and its' dependence on context (PAPERNAK). Second I will expand beyond 1D tuning functions using computational models which introduces high-dimensional stimulus spaces, the curse of dimensionality, and optimization approaches to circumvent it (MODELLING SECTION). Finally, I will apply all of this through an experiment which applies optimization techniques from machine learning to a neural population for adaptive stimulus selection(MAPS).

1.1 The Visual Heirarchy

The mammalian visual system is grossly organized hierarchically (Felleman and Van Essen, 1991; Barone et al., 2000; Batardiere, 2002). Light first enters the retina and activates photoreceptors (Field et al., 2010), then this information propagates through the LGN of the thalamus to V1. From V1, the information travels down the visual cortex posterior to anterior, through areas V2, V3, V4 and into Inferior Temporal cortex (IT) (1.1).

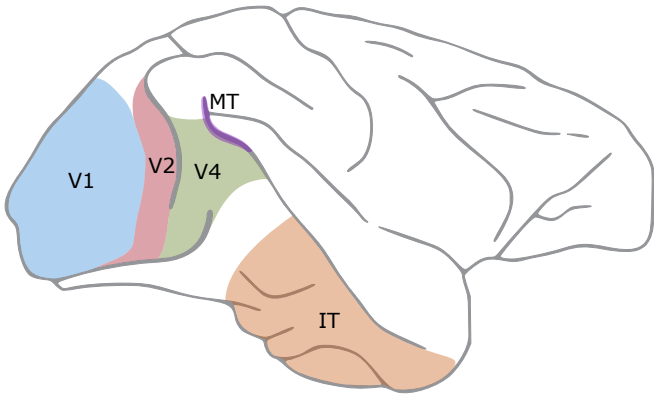

FIGURE 1.1: *The Rhesus Macaque Visual Hierarchy.* Each area depicted here is distinct in cytoarchitecture and maintains a complete retinotopic map. Information flows from the LGN (not shown) to V1, then V2, V4, and finally the inferior temporal cortex (IT) in what we call the Ventral stream.

It is known that each of these brain regions are unique and self-contained stages in hierarchical information processing. One reason they are thought to be unique stages is because each area has a full representation of the visual field (Retinotopic map) (Felleman, Xiao, and McClendon, 1997). It has also been shown that neurons in these brain areas respond differently to the same visual information (Mahon and Valois, 2001), and have different functional architecture (Yoshioka, Dow, and Vautin, 1996; Hubel and Wiesel, 1965). At each stage of the hierarchy, the visual information is processed in increasingly complex ways. Information in photoreceptors is quite simple: it consists of how many photons of light there are at each point in the visual field. The retinal ganglion cells (RGCs) then sum that information and describe the first spatial derivative of the photoreceptors, where the changes in the concentration of light are (i.e. contrast

edges) Wiesel, 1959. The simplicity of this intra-areal computation is contrasted by the more intricate transformations between brain areas. For example, Hubel and Wiesel demonstrated that neurons in V1 respond dynamically to the orientation of a bar of light Hubel and Wiesel, 1959, and so their firing rate contains information about orientation. Knowledge about the neural activity reduces the uncertainty about the stimulus and vice-versa. This stimulus-response relationship is the prototypical sensory coding function called a tuning curve. Studies have shown that the amount of stimulus information represented in the tuning curve of a neuron is highest at the peak (the stimulus that causes the highest firing rate) and the peak of the first derivative (largest slope), depending on the noise present in the system Butts and Goldman, 2006. Investigations into the neural code of the visual system therefore need to find stimulus dimensions that result in steep tuning curves and large peak responses from neurons. While bars of light are sufficient to investigate the neural code in early visual areas, these same stimuli are too impoverished to excite neurons in later areas. The low response rates are obstacles to describing the response function of neurons higher up in the visual hierarchy, like V4. The goal is still to find the domain in stimulus space that results in substantial, dynamic responses from a neuron, but the dimensionality of the stimulus space is astronomically larger. In the same manner that Hubel and Wiesel manipulated the width/orientation of a bar of light to excite V1 neurons, researchers have been developing novel strategies to make stimuli better suited for neurons in other visual areas Hubel and Wiesel, 1959; Pasupathy and Connor, 2002; Ponce et al., 2019; Cowley et al., 2017a. The resultant stimuli can be roughly categorized by the order of the underlying image statistics: first, second, and high-order. It is a precarious endeavor to match the complexity of a stimulus to the intricacy of a brain area's tuning preferences, but decades of work have guided a growing, cohesive understanding of stimulus-response functions. This work has lead to substantial improvements in sensory models of the brain as well as fundamental coding principles that generalize beyond the visual system.

1.1.1 Subsection 1

1.2 The Neural Response Function

In its simplest form, one can consider neurons to be a biological implementation of some unknown function of a stimulus parameter (θ):

$$NeuralResponse = f(\vec{\theta}) \tag{1.1}$$

The neuron takes in inputs from dendrites, and produces an output in the form of action potentials (spikes). Computational neuroscientists then try to understand how the brain processes information by studying the input-output relationship of these functions. We begin with a single neuron, and a single variable input (θ), to build the foundations for more high-dimensional cases later.

1.2.1 Tuning in One Dimension

The prototypical representation of a neurons input-output function is the tuning curve. Tuning curves are estimated by taking discrete samples along a single feature dimension (orientation for example) and plotting the neural responses against the stimulus parameter (Figure 1.2A). In this case, each dot represents one trial of the stimulus-response function, and by averaging across trials we get an estimate (dotted line) of how a neuron responds to that stimulus dimension (θ). This process provides the expected response of a neuron to each part of the stimulus space (Figure 1.2B) under the assumption that the tuning function is smooth where not sampled (**CITE FOR SMOOTH TUNING**).

Importantly, this method also provides the reliability of the neural response function. While neurons are believed to respond in a deterministic manner, the presence of uncontrollable variables (biological noise, network oscillations, latent factors, etc. **CITE ALL OF THESE**) makes most neurons appear to behave somewhat stochastically. That is, on any given trial, it may respond more or less than expected, which we call response variability. Tuning and variability both impact information signaling in unique ways, with different implications for the brain.

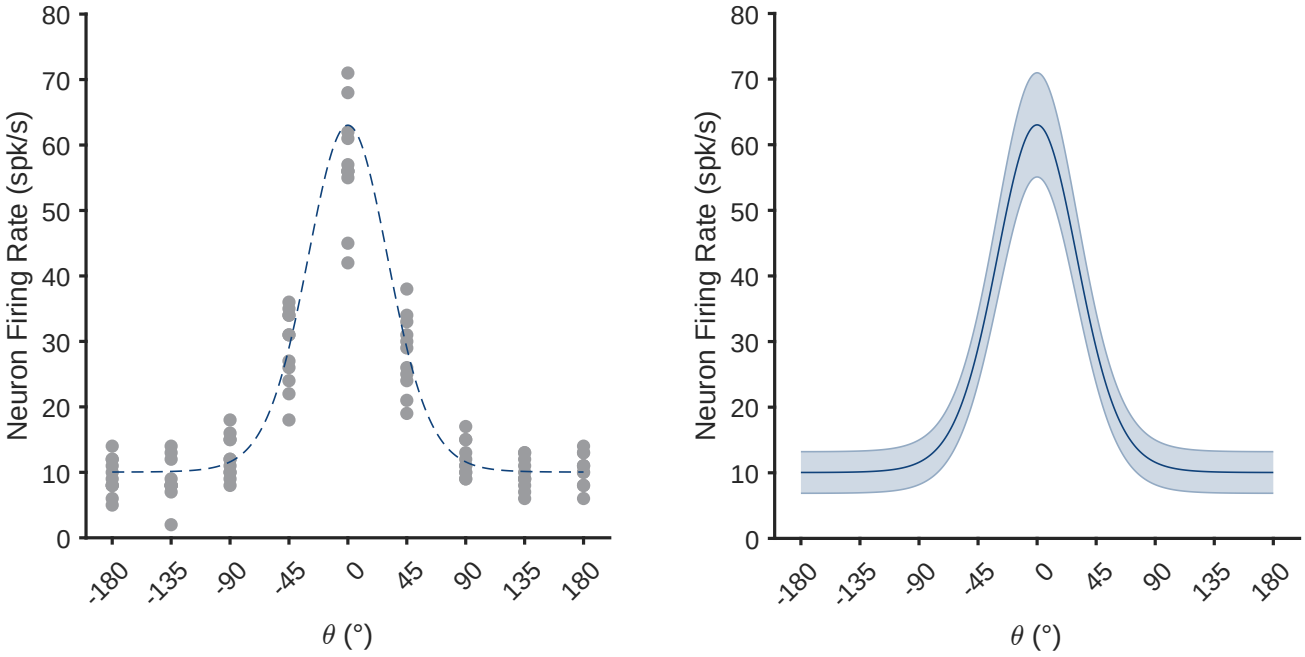

FIGURE 1.2: *Calculating a 1D Tuning Curve.* A.) The process for estimating a single neurons tuning curve to a single stimulus parameter θ. Discrete stimulus values were chosen ($-180°by45°to180°$) to span the stimulus space, and repeatedly presented (Gray dots). This provides the expected response to a given stimulus value (dotted line) for the neuron. B.) The estimated tuning and variability for the neuron in panel A.

A neurons tuning curve contains information. That is to say, knowledge of a neurons firing rate reduces uncertainty about the state of the world. Take the neuron from Figure 1.2 for example. If the neuron is firing at $40\frac{spk}{s}$, it is pretty unlikely that the stimulus is either 0° or 180°, so it is conveying information about the stimulus to other neurons. The question then becomes, *how much* information is a neuron signaling. This quantity is directly related to three main components:

1. Response Range
2. Shape of tuning curve
3. Response Variability

The first point is mitigated through natural upper and lower bounds. Neurons cannot have a negative firing rate, and neurons cannot fire arbitrarily fast due to biochemical constraints such as repolarization of chemical gradients (**CITE**), refractory periods

(**CITE**), etc. The final two points are intertwined due to quantization of response and precision of readout. Neurons cannot fire half a spike, so a single neuron cannot encode to arbitrary precision (e.g. 45° vs 45.000001°; remember that firing rates are bounded), even with 0 response variability. This makes properly utilizing the available range essential, i.e. the shape of the tuning curve.

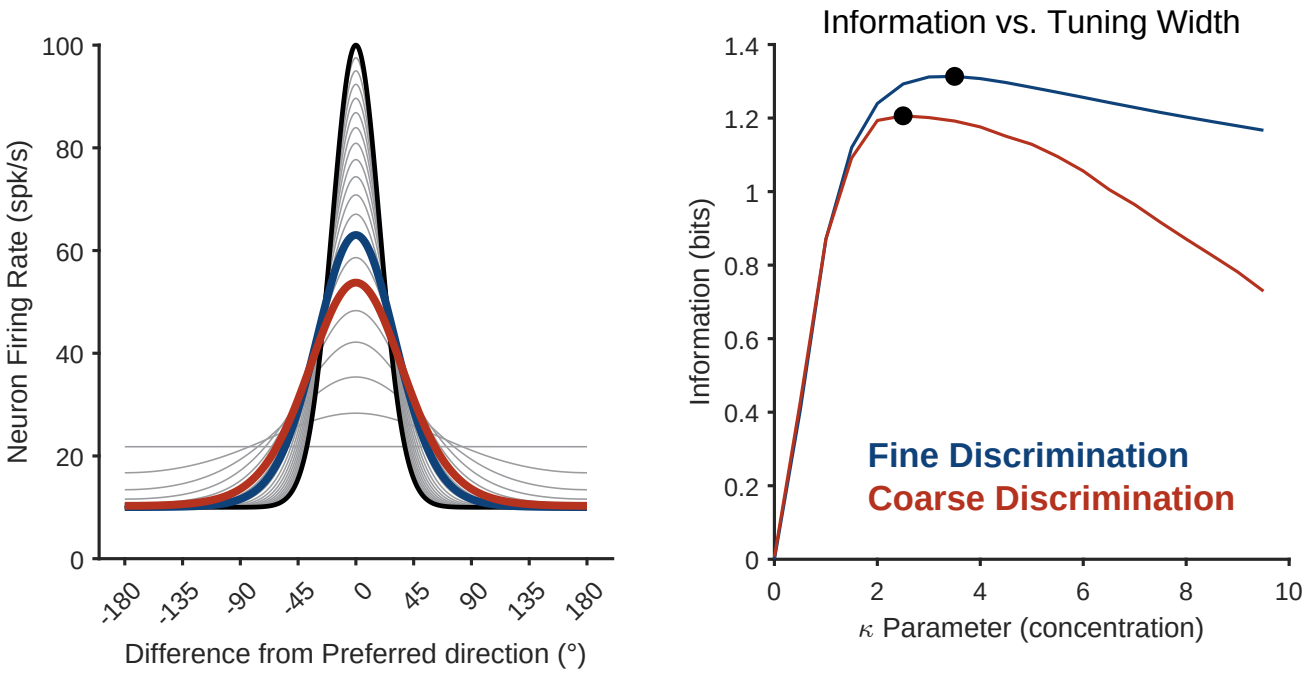

FIGURE 1.3: *Tuning curves and Information.* A.) Von Mises tuning functions with different concentration parameters (κ). Color indicates highest information tuning functions for fine (Blue) and coarse (red) discrimination. B.) Mutual information (Firing Rate and orientation) as a function of κ. Blue line depicts 1° discrimination, Red line depicts the more realistic situation of 8 stimulus classes (0° to 315° in 45° steps).

Previous work has demonstrated that the most informative parts of a tuning curve is where the slope is highest (Seriès, Latham, and Pouget, 2004). A small change in the stimulus results in the largest change in the response, making those sections the most sensitive to the stimulus dimension. Given this, one may fall into the trap of thinking larger slope means more information. Consider instead the black tuning curve in Figure 1.3A. If the task is to discriminate between $\theta = 45°$ and $\theta = 90°$, this is the worst stimulus-response function to use. In fact, the shape of a neurons tuning curve has been shown to vary with the demands on the system (**Scott2022**). In the case of tuning width

(κ parameter of a Von-Mises function), course discrimination (0° vs. 45°) necessitates a wider tuning function than fine discrimination (0°*vs*.1°; Figure 1.3B). This is because we are optimizing the tuning function for discrimination across the whole available range of θ, not just the high-slope regions.

1.2.2 nD Stimulus Spaces: Multiple Features

In the previous section I discussed the basics of tuning in 1 dimension. This explored how one neuron responds to changes in one stimulus parameter θ. This is an oversimplification of the true process, as no true stimulus can be described with only a single number. In this section I will expand the concept of a 1D tuning curve to an nD tuning surface spanning multiple feature dimensions.

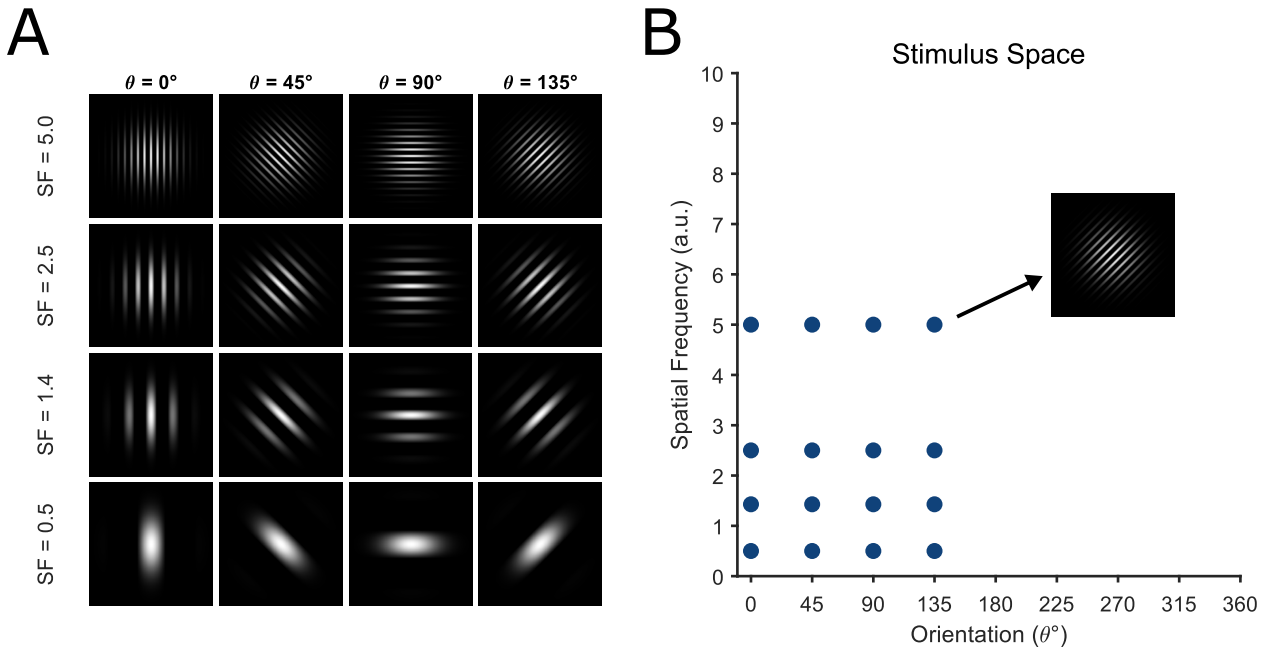

FIGURE 1.4: *Gabors as points in a 2D Stimulus Space.* A.) examples of Gabor stimuli with various θ and spatial frequency values. B.) Positions of the Gabors depicted in panel A within a 2-Dimensional stimulus space.

One of the most heavily-studied and simplest stimuli used in studies of visual neuroscience is the Gabor (Figure 1.4A). Gabors (or wavelets) are esentially oscillating light and dark patches at an orientation. These stimuli are often used in low-level visual areas such as LGN (Mahon and Valois, 2001), V1 (Bredfeldt and Ringach, 2002; Lennie,

Krauskopf, and Sclar, 1990; Tanigawa, Lu, and Roe, 2010), V2 (Liu et al., 2020) and Middle Temporal Area (MT) (**CITECITECITE**). Most such studies use the orientation dimension to produce tuning curves as described previously (Figure 1.2A), but many make necessary choices which limit them along non-studied feature dimensions (eg. spatial frequency, color, size, etc.). Let us begin with a 2D feature space by adding spatial frequency to orientation. Figure 1.4A demonstrates how independently varying the two feature dimensions results in a set of stimuli that a particular neuron may be tuned for. These are of course discrete steps representing two continuous feature dimensions (orientation and spatial frequency). This results in an important conceptualization, the stimulus space (1.4B). Here, every possible combination of orientation and spatial frequency are represented as points in a plane.

This is a natural progression from the 1-Dimensional orientation case shown before. All experiments investigating orientation tuning, necessarily limit stimuli along other dimensions. So while spatial frequency (for example) is kept constant in those experiments, neurons are still responding according to their n-dimensional tuning function. This is depicted in figure 1.5. Here we have the same model neuron from 1.2, where it's tuning before was just a slice through some 2D surface.

This idea of multidimensional tuning is both more realistic, and more problematic. One of the biggest problems with studying neuron behavior this way is how intractable it is in 3+ dimensions. Take the 1D tuning curve in 1.2A. An experimenter must test the neural response function at several points to get an estimate of the tuning curve (in this case 8 orientations), because we do not know a priori which values along the stimulus dimension any one neuron is sensitive to. If, for example, we took the neuron from 1.2A and only sampled $\pm 90^{\circ}$, we would conclude that the neuron is not tuned to orientation. This is to say there is a minimum required sampling of each stimulus dimension we are interested in. Additionally, neurons perform nonlinear operations so we must sample each relevant dimension independently. This means to get a meaningful tuning curve for an N-dimensional feature space requires around 8^n individual stimuli (assuming 8 sampled values for each dimension) sampled with repetition (5-10 trials each). So for a

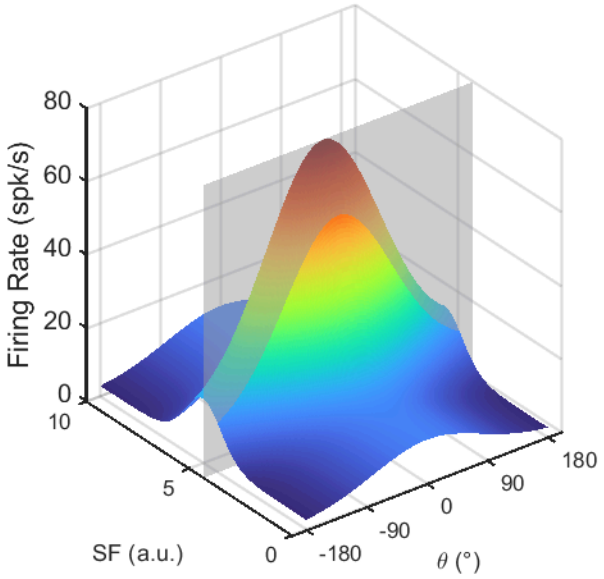

FIGURE 1.5: *Tuning along multiple Feature Dimensions.* A neurons tuning curve, in 2 dimensions becomes a tuning surface. Grey plane represents the spatial frequency value at which the tuning for θ matches figure 1.2.

Gabor stimulus with feature parameters 1.) Orientation, 2.) Spatial Frequency, 3.) Color, 4.) Contrast, and 5.) Size, with the minimum 5 trials each, an experimenter would have to show 163,840 stimuli in a single recording session. This is of course just for Gabors, one of the simplest visual stimuli. In more naturalistic settings, the number of feature dimensions could count in the hundreds. This problem motivates a more intelligent approach to searching for high dimensional feature tuning, which I will expand on in Chapter 3.

1.2.3 nD Response Spaces: Multiple Neurons

In the last section I built on the 1D neural response function by introducing the idea of multiple input dimensions: multiple features. In this section I will bring it back to 1 feature dimension, and discuss the implications of multiple response dimensions: multiple neurons.

Take again the example of neurons in V1 that are tuned for the orientation of a Gabor. This time we show a population of 8 neurons with equally-spaced preferences for

θ (Figure 1.6A). We can assume for the moment that each neuron independently contributes information about the value of θ with its' firing rate. A brain area or decoder with knowledge of all 8 neurons firing rates can accurately estimate θ. For example, if neuron 1 has a low firing rate, and neuron 2 has a high firing rate, θ is most likely to be around 0°.

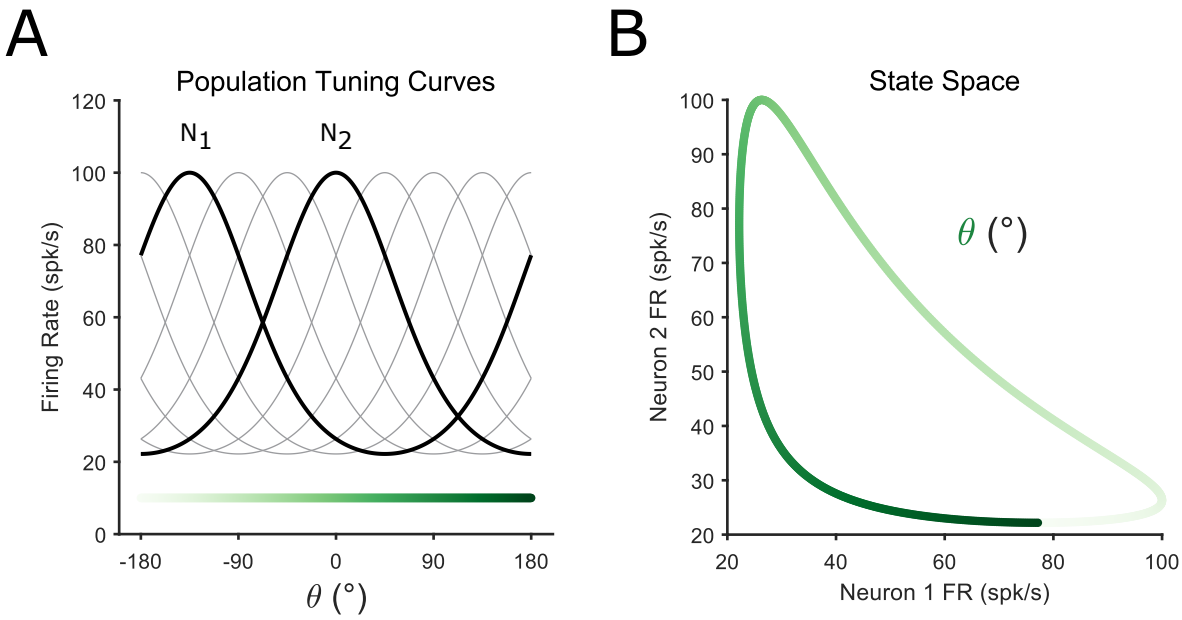

FIGURE 1.6: *Population Codes* A.) Tuning curves for 8 homogenous model neurons along the orientation feature dimension. Color at the bottom represents the values of θ. B.) A 2-Dimensional state space plotting the responses of neurons 1&2 from panel A. Color represents the value of θ that lead to each pair of neural responses.

This brings up another important concept that parallels the stimulus space from figure 1.4B, the Neural state space (Paninski et al., 2010; Cross et al., 2021). A state space is a representation of neural data in which each dimension (or axis) is the firing rate of one neuron (Figure 1.6B). We can then plot experimental variables (eg. stimulus features) according to the neural activity they resulted in. In figure 1.6B, I've plotted θ according to the relative responses of neurons 1 and 2 from panel A. This plot also represents the simplest case of a 1-Dimensional response manifold (Kriegeskorte and Wei, 2021; Chung, Lee, and Sompolinsky, 2018). The "1D" comes from the fact that we are only plotting a single feature dimension (θ).

An important point to make here, as discussed in Kriegeskorte and Wei (2021), is that tuning curves (Figure 1.6A) determine the shape of the neural manifold (Figure 1.6B), but not the other way around. Different sets of tuning curves are capable of generating the same manifold geometry. This geometry is largely affected by tuning curve shapes and relative preferred stimuli (peak FR θ and how different they are across neurons). For example, if neuron 1&2 from figure 1.6A had the same tuning curve, adding neuron 2 provides no extra information. The fact that their preferences are offset is where the extra information comes from. This does not remain true when one considers response variability from before, as two identical neurons can provide multiple samples simultaneously (think one neuron with two trials, or two identical neurons with one trial).

Likewise, another major issue when expanding intuitions about tuning beyond a single neuron, are shared neural variability. When neurons co-vary together within stimulus condition, we call these noise correlations (Cohen and Maunsell, 2010; Ruff and Cohen, 2016; Snyder et al., 2014; Moreno-Bote et al., 2014).

1.2.4 Relationships Between Two nD Spaces: Neurons and Features

Chapter 2

Neuronal Modulation Depends on Context and Feature Tuning

Introduction

The MT area of monkey cerebral cortex is a well-studied extrastriate visual area known to have robust selectivity for visual motion features (Britten et al., 1992; Born and Bradley, 2005; Pasternak and Tadin, 2020). Motion signals represented by the activity of neurons in this area are important for making memory-guided comparisons about visual motion direction (Lui and Pasternak, 2011; Wimmer et al., 2016; Katz et al., 2016). Lesions of this area impair the ability to report whether the motion direction of a stimulus matched a previous example or not (Rudolph and Pasternak, 1999; Bisley and Pasternak, 2000); whereas electrical stimulation of this area can bias the behavior of an animal as though a particular direction of motion was seen when in fact no direction information had been present (Bisley, Zaksas, and Pasternak, 2001; Salzman et al., 1992; Salzman, Britten, and Newsome, 1990). These findings indicate a key role for MT in representing behaviorally-relevant visual motion information, and demonstrate that MT has an important role in task-related perceptual decisions. One open question, however, is how behavioral goals impact the neural activity in area MT during sensory (e.g., encoding/decoding of stimulus) and non-sensory (e.g., reward contingencies, decision making, etc.) periods of the task.

Area MT acts in concert with another brain area, the Lateral Prefrontal Cortex (LPFC),

in order to do memory-guided comparisons of motion direction. LPFC and MT are reciprocally connected (Ungerleider and Desimone, 1986; Barbas, 1988; Petrides and Pandya, 2006), and both are involved in memory-guided motion comparison tasks (Zaksas and Pasternak, 2006). Neurons in LPFC contain direction information during motion discrimination tasks, but this selectivity is largely attenuated when animals do not have to make perceptual decisions, or when that information is not relevant to the task (Hussar and Pasternak, 2009; Hussar and Pasternak, 2012; Hussar and Pasternak, 2013). Previous research has also found reduced trial-to-trial variability in LPFC with increased task demands (Hussar and Pasternak, 2010), suggesting LPFC neurons may be recruited to support task performance when needed. Because of the interconnected structural and functional relationship between LPFC and MT, such a change in trial-to-trial LPFC variability with task demands may be reflected in MT dynamics and altered processing of stimulus information, but this hypothesis remains untested.

To investigate this question, we measured how activity in MT covaried with the differing demands of an active task and a passive task that used physically identical stimuli. The active task consisted of two random dot motion stimuli separated by a delay, where subjects (Rhesus macaques; *Macaca mulatta*) had to report whether or not the direction of motion in the first stimulus ("S1") matched the second ("S2"). During the passive task, no perceptual decision was required, but the motion stimuli were the same. Thus, despite practically identical sensory conditions, the task demands during active and passive tasks were different. Thus, the active task can be parsed as a sequence of: stimulus encoding (S1), memory maintainance (delay period), recall and comparison (S2), and finally decision making (S2/post-S2). For sensory periods (S1/S2), We hypothesized that heightened task demands during the active task would be reflected in sharper tuning, reduced trial-to-trial variability, and/or modulation gain, in line with prior findings about selective attention to motion direction (Martinez-Trujillo and Treue, 2004; Ponce-Alvarez et al., 2013; Cohen and Newsome, 2008; Arandia-Romero et al., 2016). For the more cognitive aspects of the task (working memory, S1/S2 comparison

signals, decision making), we expected to find stronger comparison effects, signals differentiating “same" and “different" trials independent of motion direction, in the active task.

We found that the effects of heightened task demands depended on the amount of task-relevant stimulus information (e.g. direction selectivity) neurons conveyed. Specifically, we found three distinct modulation profiles for stimulus processing between the active and passive tasks: information-enhanced, information-suppressed, and information-consistent neurons. Neurons signalling enhanced task-relevant stimulus information during the active task displayed sharper tuning, and a preferential reduction in trial-to-trial variability, but no effect on comparison signals. In contrast, information-suppressed neurons displayed a flattening of their tuning curves with no effect of task on trial-to-trial variability. The third subpopulation of neurons (information-consistent), while significantly tuned to motion direction, displayed only weak effects of task on tuning or variability. Instead, the suppressed and consistent groups showed task-dependent comparison signals comparing S1 and S2. These results suggest a division of labor in area MT, separating sensory processing and cognitive effects of the task across distinct subpopulations of neurons.

Results

Three adult male Rhesus macaques (*Macaca mulatta)* performed delayed visual motion comparison tasks while we recorded neural activity in MT (Figure 2.1A). In the active task, monkeys indicated whether a second stimulus (“S2”) had the same or a 90-degree different direction of motion than a first stimulus (“S1”) by making a saccade to one of two choice dots. All three monkeys performed above chance in the active task (m201, 10 sessions: 77.79% $\pm$ 1.08% accuracy, m202, 28 sessions: 81.63% $\pm$ 0.95%, m317, 16 sessions: 85.77% $\pm$ 1.36% ; *mean* $\pm$ *Std*). The passive task, except for a different fixation point shape, was identical up to the choice window, at which time no choice target stimuli were shown and no further action was required to receive reward (Figure 2.1A).

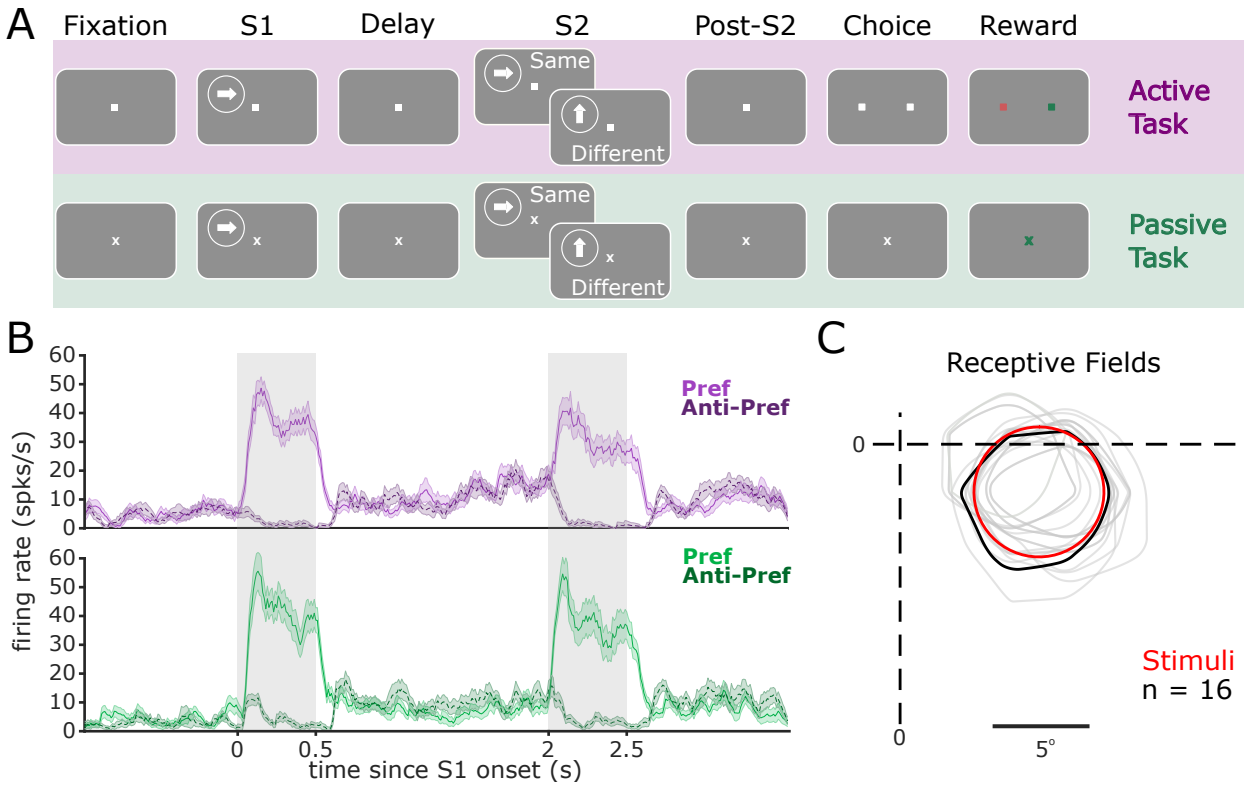

FIGURE 2.1: *Task design and task modulation of MT firing rates.* A. Trials consisted of a pre-stimulus fixation period, a first stimulus (S1), followed by a 1.5 second delay, then a second stimulus (S2) and a post-S2 fixation period. After the post-S2 fixation period subjects were either rewarded (passive task) or had to report a decision with a saccade and rewarded after correct choices (active task). Stimuli moved in one of 8 directions (0°, 45°, 90°, 135°, 180°, 225°, 270°, 315°) during S1, and then S2 was either in the same direction, or 90° off of S1 (rotated left or right). B. PSTHs of an example neuron that was recorded in both tasks. Solid line represents the neuron's response to its preferred motion direction while dashed lines indicate 180° away from preferred ("anti-preferred") C. Receptive fields (grey) of each simultaneously-recorded neuron from one example session, along with the location and size of the stimuli (red). Black curve corresponds to example neuron in B. Contours represent isointensity responses at 50% of the peak response.

Neurons were recorded with receptive field centers of 10.55 ± 0.77 Degrees of visual angle eccentricity ($mean \pm SEM$ across all neurons from all sessions; Figure 2.1C for example session). Neurons were included for analysis if: 1.) Their 50% isointensity response field (see Methods) was at least 30% covered by the stimuli, 2.) the subject did at least 10 trials in each direction condition, and 3.) they were confidently recorded across both tasks (see Methods). This resulted in 254 well-defined neurons included for analysis.

We were interested in the impact of cognitive demands on MT activity. Such demands varied over the course of a trial in the active task, including periods where stimuli were present (i.e., during S1 and S2) and also periods where stimuli were absent (i.e., pre-S1, the delay, and post-S2). For example, prior to S1, the animal should prepare cognitive resources in anticipation of the stimulus. Then, during S1, the animal must process and store task-relevant information (motion direction). During the delay, this information must then be maintained in working memory and the appearance of S2 may be anticipated. During S2, task-relevant information must again be encoded, the stored information about S1 retrieved, and a comparison judgement made. These dynamic task demands may result in varying effects on MT activity across these different stages. We first describe the effect of task demands on motion-direction signalling by MT activity during stimulus presentations (S1 and S2). Second, we will describe effects of task demands on MT activity when stimuli were absent. Third, we will describe effects of task demands on MT activity during the comparison stage of the task (S2 through decision).

Task effects in MT depend on neural tuning

We hypothesized that the accuracy of motion direction encoding in MT would improve when that information was task-relevant (i.e., in the active task compared to the passive task). To test this, we measured the mutual information (MI) between neural firing rates and the motion direction of S1 and S2. MI quantifies how much information about one signal is provided by another signal (and vice-versa), and takes into account both the

tuning of neural responses with respect to a stimulus as well as trial-to-trial response variability (Hatsopoulos et al., 1998; Quian Quiroga and Panzeri, 2009; see Methods). Across all neurons in our sample, we found similar degrees of motion direction signalling in the active and passive tasks (Figure 2.2A). As MT is a mid-level sensory area, this was unsurprising.

We hypothesized that changing task demands might be especially impactful on the activity of neurons that signal task-relevant information. That is, switching from passive viewing to a task requiring judgment of motion direction might have a particularly strong effect on neurons strongly signaling motion direction compared to neurons that did not signal that information so strongly. To test this hypothesis, we calculated the task effect of motion information for each neuron by subtracting the timeseries during the passive task from the active task. This provided a metric which quantifies, at each timepoint, how each neuron signals motion direction information differently across tasks (Figure 2.2B). We then clustered neurons according to the Pearson distances between these task effect time-courses (see Methods). We found 3 clusters to be the most parsimonious model, and hereby refer to them as suppressed, enhanced, and consistent groups (Figure 2.2B&C), which describes the average task effect on direction information for neurons within each cluster.

We found it interesting that a substantial group of neurons displayed a marked reduction in MI during the active task (suppressed), as it represents a detriment in the population of neurons for direction coding. Taken together with the enhanced neurons, which followed the expected pattern of improved direction signalling, these results suggest that heightened task demands result in task-relevant information becoming disproportionately represented in a smaller number of highly-informative neurons.

Heightened Task Demands Differently Impact Tuning for Subpopulations of Neurons

We found that mutual information between neuron firing rates and motion direction changed when motion direction was task-relevant (active task) compared to when it

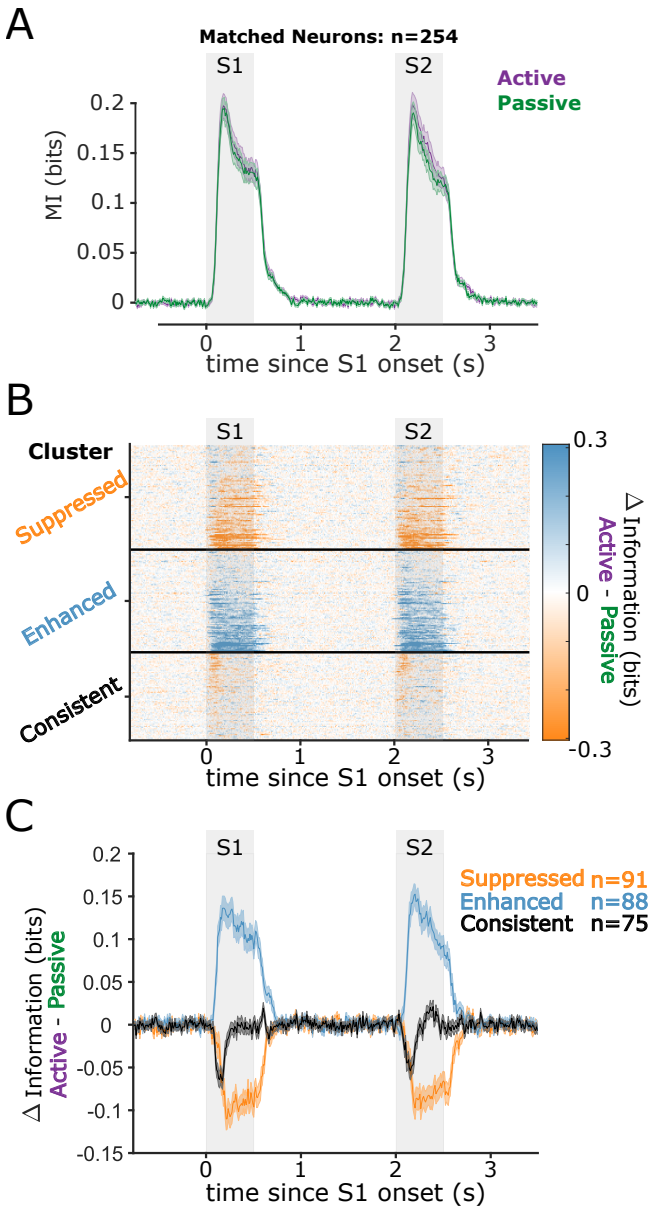

FIGURE 2.2: *Motion Information Clustering.* A.) Time course of mutual information between matched neurons firing rates' and motion direction in the active and passive task. B.) Time series for active minus passive motion information (MI) within neuron. Each row is a single neuron matched across task, and color represents the difference in information. See Methods for clustering algorithm. C.) Within-cluster averages from panel B.

was not (passive task). Since MI takes into account both stimulus tuning and trial-to-trial variability, the observed changes in MI could be consistent with a change in tuning, a change in trial-to-trial variability, or a mixture of both. To better characterize the nature of the task-demand effects we found, we separately analyzed tuning and trial-to-trial variability for enhanced, suppressed, and consistent neuron groups.

We tested for differences in tuning for each group by calculating the average firing rate for each neuron, and compared effects of task, direction condition, and stimulus (3-way ANOVA: Figure 2.3A-C). The main effect of 'stimulus' (S1 vs S2) was negligible for each group (enhanced: $p = 0.238$; suppressed: $p = 0.187$; consistent: $p = 0.531$), so for visualization purposes we plotted S1, which unlike S2 does not have concurrent comparison processes. We found the expected pattern of tuning modulation for enhanced neurons, with gain around preferred direction and suppression to 180 degrees off preferred, supported by an interaction effect between task and direction ($p \approx 0$: Figure 2.3A). In contrast, the information-suppressed group showed a reduction in response around their preferred stimulus in the active task (Figure 2.3B). Interestingly, the consistent group shows a slight increase in response to anti-preferred motion (180deg off pref) which results in a flattening of their tuning curves (task effect: $p = 0.005$). This means that during the active task, neurons that had suppressed or consistent information had flatter (broader) tuning profiles, which in isolation would constitute a deficit to direction coding when that information is task-relevant.

Trial-to-Trial Response Variability is Modulated by task and Stimulus Features

In addition to tuning, MI also takes into consideration trial-to-trial variability in responses. we reasoned that the task effects on MI may be partially due to altered variability of neural responses. To test this, we calculated the entropy of neural responses (separated again by task, motion direction, and stimulus, 3-way ANOVA) and normalized measurements relative to those of a simulated Poisson process matched for intensity (entropy factor (HF); see Methods).

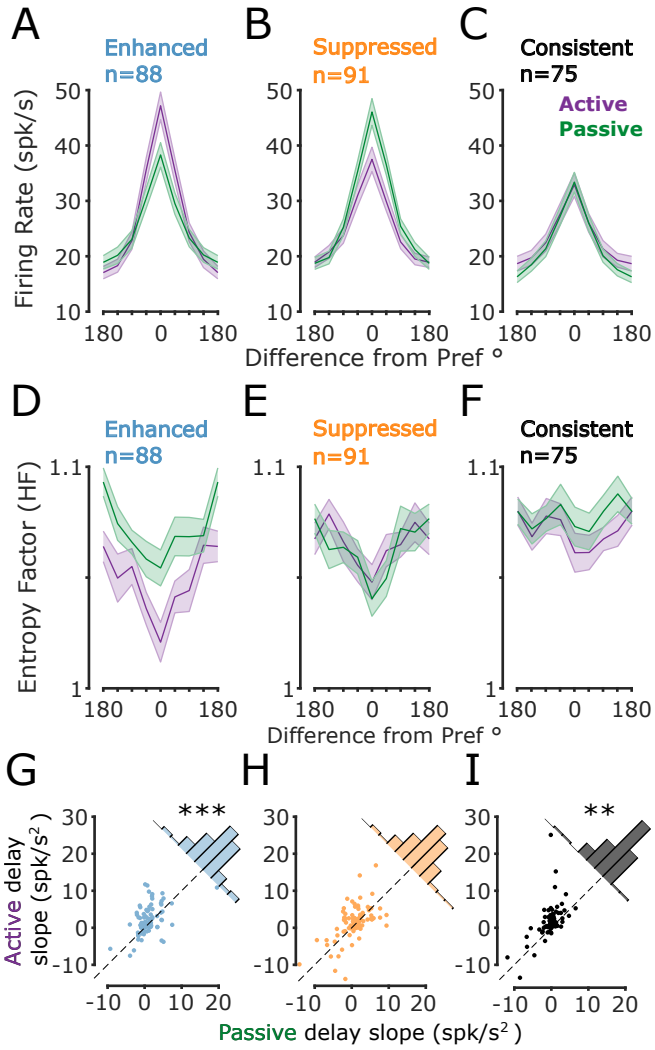

FIGURE 2.3 *Effects of task demands differed depending on how informative a neuron was about task-relevant information.* A.) Average Tuning Curves for information-enhanced neurons during the active (purple) and passive (green) tasks. Both curves contain the same neurons. Error bars are $\pm SEM$ across neurons.B-C.) Same as A for information-suppressed and consistent groups respectively. D.) Average trial-to-trial variability during S1 quantified with HF (See Methods). E-F.) Same as panel D for information-suppressed neurons and consistent groups respectively. G.) Slope of a linear fit to enhanced neurons' firing rates vs time during a 1s interval before S2 onset in the Active vs Passive tasks. There was a significantly higher ramping during the active task (***: $p = 5.66 \cdot 10^{-5}$, t-test). H-I.) Same as panel G for information suppressed (ns) and consistent (**: $p = 0.0098$) groups respectively.

We found an overall reduction in HF in the active task, relative to the passive task for information-enhanced neurons ($F = 60.24, p \approx 0$; Figure 2.3D). Additionally, all three classes of neurons had a reduction in trial-to-trial variability that was a function of motion direction (enhanced: $F = 6.64$, $p \approx 0$; suppressed: $F = 6.97$, $p \approx 0$; consistent: $F = 2.07$, $p = 0.044$; Figure 2.3D-F). Neurons had the largest reduction in HF to their preferred stimuli, with weaker effects as motion direction diverged from this direction. The preferential reduction in variability was strongest in the information-enhanced group, consistent with the improvement to both tuning and MI. No active vs. passive task effect was found for the information-suppressed group, though they did still display an effect of motion direction on HF that was consistent with the enhanced neurons. Information-consistent neurons showed a weak improvement in HF that likely counteracted the weak detriment in tuning, resulting in the net zero change in motion direction information that classifies the group.

To summarize, all three groups of information-modulated neurons displayed different patterns of tuning and variability modulation, which further supports our hypothesis that these groups of neurons differently contribute to the task.

Task Demands Modulate MT Firing Rates During Non-stimulus Periods

We next turned our attention to the effects of varying task demands on MT activity during periods when dot motion stimuli were absent (pre-S1, during the delay between S1 and S2, and post-S2). Because no stimuli were present, effects during these intervals would be due only to cognitive processes (e.g., anticipation of S1 or maintenance of memoranda during the delay). The pre-S1 period was highly predictable in this task (1000ms post fixation), so we expected to see a gradual increase ("ramping") of firing rate during this period, reflecting anticipation. We quantified pre-S1 ramping as the slope of a linear fit to FR vs. time during a one second window before S1 onset. We found a significant task effect of pre-S1 ramping only within the information enhanced group (T-test Passive minus Active slopes: $p = 1.02 \cdot 10^{-4}$).

Next we considered the delay period between S1 and S2. Because the timing of this delay was also highly predictable in our task (always 1.5 seconds), animals could anticipate the appearance of S2. We also found significant ramping during the delay period for enhanced neurons ($p = 5.66 \cdot 10^{-5}$) and consistent neurons ($p = 0.0098$), where both groups had higher delay ramping in the active task (Figure 2.3G-I). This increased ramping in the active task may reflect additional task demands related to the preparation of the S1 and S2 comparison. We also asked whether MT activity might continue to be selective for the motion direction of S1 during the delay, which could be consistent with a working-memory-related maintenance process. However, we found that MI between MT activity and S1 motion direction rapidly fell to levels consistent with the null hypothesis after S1 offset, and this did not differ based on task demands (Figure 2.2A).

MT Activity is Affected by Cognitive Aspects of Memory-guided Visual Comparisons

During S2 of a given motion direction, our active task required subjects to make a saccade to the right if the direction of the preceding S1 was the same ("same trial"), and a saccade to the left if the direction of the preceding S1 was different ("different trial"). It has previously been observed that MT neurons' responses to physically identical S2 stimuli differed whether they came from "same" or "different" trials, which we termed a "comparison effect" (Lui and Pasternak, 2011; Zaksas and Pasternak, 2006). Here we ask: (1) are CEs different in the active versus the passive task (when no comparison is needed); and (2) is the task-modulation of CEs (if any) different across the three neuron groups (enhanced, suppressed, consistent)?

We calculated comparison effects as the area under the receiver operating characteristics curve (AUC) within direction condition during S2, between "same" and "different" trials (Figure 2.4A). We expected that the cognitive effects of the task may run orthogonal to the sensory improvements (i.e. stronger comparison effects in non-enhanced groups), and this would be indicative of a division of labor. We indeed found that

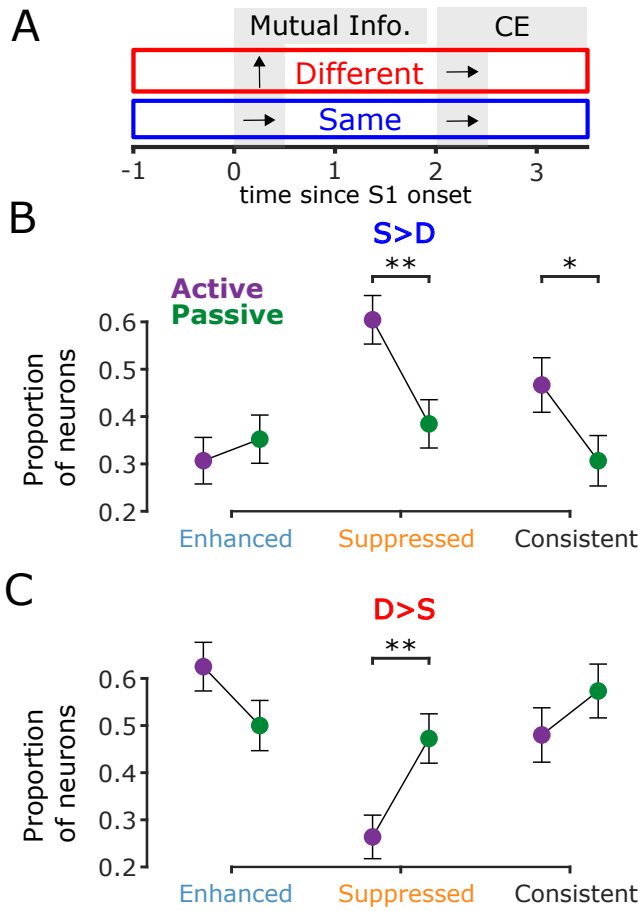

FIGURE 2.4: *Recruitment of MT neurons for cognitive aspects of the task* A.) Schematic of comparison effect analyses. Neurons were classified into groups according to their Pearson distance during S1 and the Delay. Comparison effects were then calculated from S2 onset up to the appearance of the choice targets. B.) Proportion of neurons within each information group with significant $S > D$ signal at some point during the CE window in panel A. C.) Same as panel B for $D > S$ neurons.

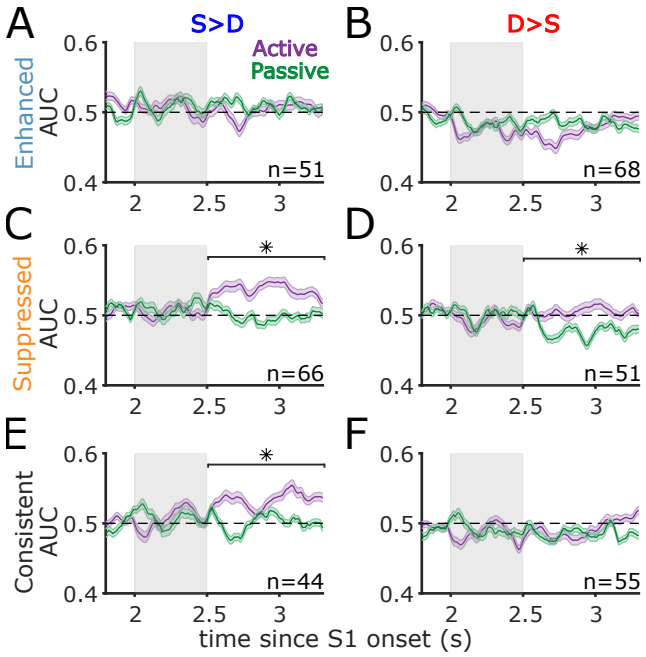

FIGURE 2.5: *Comparison Effects increase from stimulus to decision* A.) Time course of comparison effects (AUC between same and different trials within stimulus type) for neurons that were information-enhanced and significantly $S > D$ in either task. B.) Same as panel A but for information-enhanced $D > S$ neurons. C-D.) Same as A-B but for information-suppressed neurons. E-F.) Same as A-B but for information-consistent neurons. *: $p < 0.05$ for the difference between tasks over the indicated interval.

information-suppressed and consistent groups showed a significant increase in the number of $S > D$ neurons with no effect in the information-enhanced group (Figure 2.4B; Suppressed: $\chi^2 = 8.79, p = 0.003$, Consistent: $\chi^2 = 4.05, p = 0.044$). Interestingly, the suppressed group show a reduction in $D > S$ neurons in the active task (Figure 2.4C; Suppressed: $\chi^2 = 8.53, p = 0.0035$). An important point to note here, is that the same proportion of significant neurons in all three information groups shows CEs during the passive task, and the active task influenced their cognitive contributions differently.

We next looked at the time courses of comparison effects from S2 through appearance of the choice dots (Figure 2.5), again separated by information-group and direction of CE. These time courses reflect the aforementioned division of labor, where the information-suppressed and consistent groups contribute to the cognitive aspects of the memory-guided comparison (Figure 2.5C-F), while the information-enhanced group

does not (2.5A-B). So, in addition to a higher proportion of neurons signalling CEs, the average CE signal ($S > D$) during the post-S2 window also increased with heightened task demands (Figure 2.5C Kolmogorov-Smirnov test: $p = 1.11 \cdot 10^{-5}$; Figure 2.5E Kolmogorov-Smirnov test: $p = 8.22 \cdot 10^{-4}$). The higher proportion of $S > D$ neurons in the suppressed and consistent groups, along with their increased CE signalling, indicates that while these groups did not improve stimulus encoding with heightened task demands, they were recruited to aid with the comparison of S1 and S2.

Discussion

We hypothesized that neurons in the primate Middle Temporal Area (MT) area behave differently when task demands increase in order to improve information processing for goal-oriented behavior. We tested this hypothesis by recording activity of MT neurons in monkeys performing two tasks, one active and one passive. We found that in the active compared to the passive task, (1) three patterns of task effects on information signalling arose that were distributed across subpopulations of neurons, and (2) sensory and cognitive aspects of the tasks are handled separately by these subpopulations.

We found that firing rates of neurons in MT contained direction information during the stimulus periods (Figure 2.2A), and that increasing task demands had one of three broad effects on motion information for each neuron: information-enhancement, information-suppression, or information-consistent effects (Figure 2.2B). We then asked whether the changes in mutual information (MI) were caused by tuning or variability. However, the extent to which tuning and variability are each influenced by cognitive factors has been a subject of intense research (Renart and Machens, 2014; Gilbert and Li, 2013), and each has different implications for computation and neural mechanisms. To better characterize the role of task demands on motion direction signaling in MT in the context of this prior work, we separately examined tuning and variability. As the neurons were matched across task, we could directly compare how each neuron responded to motion in the active and passive conditions. Information-enhanced neurons showed sharper tuning curves with larger responses to their preferred motion direction and

a suppression to anti-preferred (Figure 2.3A). Information-suppressed neurons on the other hand, displayed a marked reduction in response to their preferred stimulus in the active task, resulting in the detriment to MI observed. As a result, these neurons became less tuned for motion direction when that information was more task-relevant. These effects on tuning are consistent with the classification of neurons based on changes to motion direction signalling in MI, but may not account for the full picture, as MI is also affected by trial-to-trial response variability, which we examined next.

By measuring entropy factor (HF), we found a strong relationship between direction preference and variability, which did not depend on group (Figure 2.3D-F). Neurons had the largest reduction in trial-to-trial variability during presentations of their preferred stimulus, with weaker effects as direction diverged from preferred. This cannot be due to the increased firing rate for those directions, as HF accounts for rate effects (see section Methods), and a rate confound would result in the opposite trend (that is, typically variability is biased downward for lower rates, but we found higher variability at lower rates; Churchland et al., 2010). The effect of heightened task-demands in the active task was largest for the information-enhanced neurons, which compound the tuning-based improvements to MI (Figure 2.3D). Interestingly, suppressed neurons showed no effect of task on variability, whilst maintaining the effect of motion direction. This means that heightened task demands flatten the tuning curves of these neurons, without altering the trial-to-trial variability. Previous researchers have suggested that a substantial portion of trial-to-trial variability can be understood in terms of neurons' susceptibility to changes in cognitive state (Ecker et al., 2016; Denfield et al., 2018); thus one interpretation of this pattern of results is that these neurons decrease their participation in sensory processes (reduced tuning) while maintaining their participation in more cognitive processes (consistent trial-to-trial variability) The reduction in trial-to-trial stimulus response variability we observed in enhanced neurons when task demands were elevated is reminiscent of the finding of Mitchell, Sundberg, and Reynolds (2007), who found general reductions in Fano Factor in V4 responses when animals selectively attended to a stimulus compared to when that stimulus was not attended. The novel and

more surprising result we found is that the strength of variability reduction depended on whether the stimulus was preferred (great reduction in variability) or less-preferred (less reduction in variability). This suggests that one effect of elevating task demands is a preferential improvement to information transmission reliability according to neurons' feature tuning.

We found significant changes in non-stimulus firing rate (FR) in the active task compared to the passive task, such as larger FR ramping during the delay period (Figure 2.3G-I). Ramping of neural firing rates has traditionally been explored in the context of motor preparation (Ding, 2015; Narayanan, 2016), and decision making (Shadlen and Newsome, 2001), where it has been typically linked to anticipation. Finding anticipatory increases in firing rate for sensory neurons in MT is interesting, and is not likely explained during the pre-S2 interval of our tasks through either decision making or motor planning, as neither a correct decision or appropriate motor plan can be made before first seeing S2. More likely, the ramping we observed is related to preparing cognitive and attentional resources for the perceptual phases of the task, which had highly predictable timing, as has also been found for LPFC neurons (Hussar and Pasternak, 2010; Bisley et al., 2004). This line of thought has also been explored in the context of another nearby visual region, V4 (Snyder, Yu, and Smith, 2018; Luck et al., 1997), where anticipatory ramping has been linked to interactions between V4 and prefrontal cortex (Snyder, Yu, and Smith, 2021). Taken together, these results suggest anticipatory signals may originate in prefrontal cortex and influence visual cortex via top-down feedback.

In addition to the more strictly sensory aspects of the task, the active task contains a comparison component which requires additional cognitive resources such as working memory. A greater response to S2 on "different" trials compared to same trials ("$D > S$") could be consistent with a response adaptation effect, while a greater response to S2 on "same" trials ("$S > D$") would be more consistent with a facilitation effect (Kohn and Movshon, 2003). We would expect that if CEs in MT are explained primarily by adaptation/facilitation, we should find similar effects in the active and

passive tasks; any task effect should indicate a greater role for memory-guided comparison processes. We found no difference in comparison effects for information-enhanced neurons but significantly more extreme comparison effects for the suppressed and consistent groups (Figure 2.5). These cognitive effects being isolated to neurons that became worse at signalling motion direction when that information became more task-relevant further supports a division of labor in area MT for completing the task. We found that comparison effects emerged most clearly during the period after the offset of S2 and before the execution of the response saccade (the 'post-S2' interval). This underscores the non-sensory, cognitive nature of these effects (since the sensory stimulus was absent when effects were strongest), and reduces the potential that response adaptation or repetition suppression could explain D>S comparison effects (Lui and Pasternak, 2011; Kohn and Movshon, 2003). This relatively late time-course of comparison effects in MT differs from earlier reports, which found comparison effects emerging shortly after S2-onset (Lui and Pasternak, 2011; Zaksas and Pasternak, 2006). One reasonable explanation for this difference in the timing of comparison effects across studies is the difference in timing between the onset of S2 and the animals' reports. Earlier studies required the animals to respond immediately following the offset of the S2, whereas in the current study animals must withhold responding until after the post-S2 delay. Thus, if the timing of comparison effects was more tightly related to the animals' reports than to the time of S2 onset, then that would be consistent with the results across all these studies of comparison effects in MT and further underscores the cognitive role of comparison signals. Finally, in earlier studies decisions were reported with a manual button press (Lui and Pasternak, 2011; Zaksas and Pasternak, 2006), whereas the current study required animals to report with a saccade, reinforcing the notion that comparison effects are related to cognitive decisions rather than the formation of particular motor plans.

Class	Tuning			HF			Delay Ramping	CE
	Task	Dir.	Stim.	Task	Dir.	Stim.		
Enhanced	***	***	ns	***	***	*	***	ns
Suppressed	***	***	ns	ns	**	*	ns	**
Consistent	**	***	ns	**	*	*	**	*

TABLE 2.1: Task effects summary. Significance of task effects separated by information clusters (*: $p < 0.05$, **: $p < 0.01$, ***: $p < 0.0001$, ns: not significant). Statistics for Tuning and entropy (HF) were a three-way anova between task, motion direction, and stimulus (S1 vs. S2). Comparison Effects (CE) were χ^2 tests between the active and passive tasks (2.4B). Delay ramping was compared using t-tests on the slopes (Passive minus active: (2.3 G-I).

Conclusion

In the present study, we investigated the effects of task demands on information processing in area MT of the macaque. We found substantial differences in variability and tuning profiles depending on the degree to which a neuron represented task-relevant information in its firing rate. In addition to these sensory components of the task, MT neurons also show stronger cognitive signalling with heightened task demands, such as anticipatory ramping and heightened comparison effects. These results highlight the role of MT populations in all phases of memory-guided comparisons of visual motion direction, and, combined with the previous findings in Lateral Prefrontal Cortex (LPFC), suggest a continual interplay between prefrontal and extrastriate visual cortical areas during cognitive task performance. Importantly, involvement in sensory versus cognitive processes was found to be flexibly distributed across subpopulations of MT neurons, with some neurons taking on greater sensory signaling when task-relevant, and other neurons shedding sensory selectivity in seeming favor of greater cognitive responsibilities.

Methods

Resource Availability

Lead Contact

Requests for further information should be directed to the lead contact Adam Snyder (adam.snyder@rochester.edu).

Materials Availability

This study did not generate any new reagents.

Data and Code Availability

Data and code used for this paper are made available by request through the lead contact.

Subjects

Subjects used in this study were three adult male rhesus macaques ages 7, 8, and 7 years, for 201, 202, and 317. All training, surgery, and experimental procedures were performed in accordance with the National Institutes of Health *Guide for the Care and Use of Laboratory Animals* and were approved by the University of Rochester Committee for Animal Research. Surgery was performed using aseptic technique with isofluorane general anesthesia and perioperative opiate analgesics. An initial surgery was performed to implant a surgical steel head holder restraint embedded in bone cement secured to the cranium with ceramic bone screws. After behavioral training, a subsequent surgery was performed to implant a PEAK canula (19 mm diameter; Crist Instruments, Hagerstown, MD) over MT.

Data Acquisition

Recording chambers enclosed the craniotomies and contained 1mm-spaced CILUX grids (Crist Instruments). Thirty-two-channel S-probes (Plexon, Dallas Texas) were lowered

through custom-made steel guide tubes, which were themselves inserted just low enough to penetrate the dura. We then drove the electrodes using a NAN electrode drive (NAN Instruments, Nof Hagalil, Israel). Recordings were done by coordinating a Plexon (Dallas, Texas) Multichannel Acquisition Processor and the data acquisition system TEMPO (Reflective Computing).

Receptive Field Mapping

Prior to each recording session, receptive fields were mapped in order to identify where the stimuli should be displayed. The initial manual phase consisted of moving a patch of dot motion around on the stimulus display with a computer mouse while listening to spiking activity via an audio monitor. Afterwards, we presented small dot motion patches (1°) in different directions on the vertices of a grid spanning the likely RF area identified in the manual step. Stimuli for each session were placed such that they covered the aggregate receptive field area for the recording (Figure 2.1B).

Stimulus Presentation

Stimuli were presented at 75 Hz monitor refresh rate on a 19-inch IIyama Vision Master Pro-513 monitor with 1,152 by 870 pixel resolution. They were 100% motion-coherence random dot kinematograms in one of 8 directions ($0°, 45°, 90°, 135°, 180°, 225°, 270°, 315°$) placed in a circular aperture fit to the size of the receptive fields, with a dot diameter of 0.03° and a density of $3\frac{dots}{deg^2}$. Dot luminance was $15\frac{cd}{m^2}$, shown on a dark background of $0.1\frac{cd}{m^2}$. Monkeys were required to maintain fixation within 2° of a central dot throughout the trial until the response interval, and eye position was monitored with an ISCAN infrared eye-tracking device.

Task Design

Trials started once subjects fixated on a central dot. They then had to maintain fixation for 1 second before S1 onset. Both S1 and S2 lasted 500ms. S1 was followed by a 1.5 second delay period, and then the second stimulus S2 was presented. Subjects then had to

wait an additional 1s after S2 offset before either a choice was required (active task), or they were simply rewarded (passive task). For the active task, the central fixation point was extinguished at the beginning of the response interval, and two identical choice targets were presented 5 degrees to the right and left of fixation, and the animal indicated its judgement as to whether S1 and S2 were the same direction or not by making a saccade to the right or left choice target, respectively. In most recording sessions, we collected data for both the active and the passive tasks. We always collected data for the active task before the passive task, because animals would have been unmotivated to perform the more difficult active task if they had performed the easier passive task first.

Data Analysis

Spike sorting was done offline with Plexon sorter (Version 3.3.2) by using Principal Component Analysis (PCA) on the spike waveforms and manually clustering. A neuron was included for analyses if there were at least ten trials in each direction condition, and if the stimuli covered at least 30% of its 50% isointensity response field. A total of 1264 neurons across both tasks passed these criteria (201: n = 263, 202: n = 454, 317: n = 547), with 928 neurons recorded in the active task and 336 neurons recorded in the passive task. Of those neurons, 254 were confidently matched across task and included for further analysis. Neurons were considered matched across task if they were recorded on the same channel and their waveforms were highly correlated ($R^2 > 0.99$). All subsequent analyses were done using custom routines for Matlab 2020a (The MathWorks, Inc, Natick, MA).

Mutual Information

Mutual information (MI) quantifies information (in bit) shared between two variables, i.e.: how much the uncertainty about one variable (motion direction condition, in our case) may be reduced with knowledge about the second variable (spike counts). MI provides a robust metric of direction selectivity that accounts for changes in tuning curves, variability, and absolute firing rates. We calculated MI using:

$$MI(x,y) = \sum_x \sum_y p(x,y) \log_2 \left(\frac{p(x,y)}{p(x)p(y)} \right) \tag{2.1}$$

Where $p(x,y)$ is the joint probability distribution between number of spikes and direction condition, and $p(x)p(y)$ is the product of marginal probability distributions. This provides how many bits of information a neuron's firing rate contains about direction and vise versa. For $p(x)$, we used the probability of observing a spike count in a bin of width Δx sp/s, where the bin width was determined by "Scott's rule" (**scottsRule**):

$$\Delta x = \frac{3.5 n^{-\frac{1}{3}}}{n} \sum_i^n (x_i - \bar{x}) \tag{2.2}$$

We calculated the mutual information between spike count and S1 direction for each non-overlapping 50ms bin from the start of each trial up to the end of the delay, and then the MI between spike count and S2 direction through the end of the trial. In order to correct for spurious effects that come from differences in trial-counts, we baseline-corrected MI by calculating it many times with shuffled conditions, and subtracted this out (Hatsopoulos et al., 1998). We then computed the bitrate by dividing this metric with the bin size (0.05s).

$$I(x;y) = \frac{MI(X;Y) - MI_{\text{shuffled}}(X;Y)}{0.05s} \tag{2.3}$$

Classification of neurons into information Enhanced, Suppressed, and Consistent subgroups

We calculated baseline-corrected mutual information (MI) between the firing rate of a neuron and motion direction shown for each time bin. From trial start through S2 onset MI was calculated according to S1 direction. From S2 onset through the end of the trial, it was calculated between firing rate and S2 direction.

We then took the MI time series for a neuron in active, minus passive, in order to get a task-effect of motion information over time. Note that this was only possible for neurons that were successfully matched across tasks (n=254). The clustering algorithm

contains 3 distinct steps.

1.) Calculate the Pearson distance (i.e., one minus the Pearson correlation) between each pair of neurons' task-effect time series. This was done on a window from trial start through the end of the delay. We did this in order to disentangle the sensory and cognitive components, since clustering on S2 would create a circularity for later analyses.

2.) Reduce the dimensionality with multidimensional scaling to five dimensions (to mitigate the "curse of dimensionality" for clustering with high-dimensional data).

3.) Model selection to pick the appropriate number of clusters. This consisted of fitting multiple Gaussian mixture models to the data, each with different numbers of components. We then selected the appropriate number of clusters by selecting the model with the lowest Bayes Information Criterion (BIC), which was three clusters.

4.) K-means clustering using the appropriate number of components (3) determined in step 3.

In this way, neurons were partitioned into groups based on how motion information signalling changed across the active and passive tasks. This allows us to then see how other task-related effects may depend on the type of information modulation a neuron receives.

Entropy Factor

Entropy Factor (HF) quantifies the entropy of a neuron's spike count (across trials) relative to a Poisson process with the same rate parameter, λ (Rajdl, Lansky, and Kostal, 2017). It is similar to Fano factor, in that a value of 1 indicates equivalence to a Poisson process, while values greater or less than 1 indicate distributions that are supra-poisson or sub-poisson, respectively. However, unlike Fano factor, which compares the variance

of a distribution of spike counts to its mean, entropy factor takes into account the entire distribution of spike counts. This provides a more reliable metric than Fano Factor, particularly when there are a low number of observations, for which sample variance is biased lower than the expected variance in the limit of infinite data. For each 50ms time bin, t, we calculated the entropy $H_{Observed}(\vec{x}_t)$ of the distribution of spike counts $(\vec{x}_t)$ across trials with the same stimulus direction and divided it by the entropy of a simulated Poisson distribution with the same intensity and number of trials.

$$HF(\vec{x}_t) = \frac{H_{Observed}(\vec{x}_t)}{H_{Poisson}(\hat{x})} \tag{2.4}$$

Here, $H_{Observed}(\vec{x}_t)$ is the entropy of the distribution of spike counts across trials $i \in [1, n]$ for a neuron at time t, defined by:

$$H_{Observed}(\vec{x}_t) = -\sum_{i=1}^{n} p(x_t^i) \log\left(p(x_t^i)\right) \tag{2.5}$$

where $H_{Poisson}(\hat{x})$ is the entropy of a simulated Poisson process with rate parameter λ:

$$\lambda = \bar{x}_t \tag{2.6}$$

The entropy of a Poisson process was calculated by doing 200 simulations of spike counts for n trials pulled from a Poisson distribution with rate parameter λ_t, and the same unbiased bins used for the data (eq. 2.2. By then averaging the observed entropies of the simulations, we get an estimate of how variable, on average, we would expect the matched Poisson process to be. This normalization accounts for bias in sample entropy due to differences in firing rate or trial count.

Tuning Curves

Tuning curves were calculated as the average firing rate during the stimulus window for each of the 8 directions. For testing the effect of stimulus (S1 vs. S2) on tuning and HF, we used a three-way ANOVA with factors of 'direction' (eight levels corresponding

to each motion direction), 'stimulus' (two levels: S1 vs. S2) and 'task' (two levels: active vs. passive).

Comparison Effects

Comparison effects (CE) were calculated as the area under the curve of the Receiver Operating characteristic (AUC). For each neuron, trials were separated by direction condition (during S2), and then by trial type (same direction or different direction trials depending on whether S1 matched S2). CE was calculated on firing rates (convolved with a 100ms smoothing kernel) for each non-overlapping 10ms bin, as the AUC between 'same' trials and 'different' trials within direction. AUC values were then averaged across direction condition within each time bin, resulting in a time course of AUC values for each neuron. Values greater than 0.5 indicates a neuron that responds more robustly to identical visual stimuli on trials where the directions of S1 and S2 matched ($S > D$ neurons), while values less than 0.5 indicated the opposite ($D > S$ neurons).

Statistical Significance of CE

Statistical significance of CE was determined using a bootstrapping procedure. Trial labels ('same' or 'different' trial) were randomly permuted, and AUC values were calculated 500 times per neuron. A neuron was considered significantly CE signalling (Figure 2.4) if its AUC was significantly different from the bootstrap distribution ($\alpha = 0.025$: two-tailed) for a significant number of time-points ($\alpha = 0.05$: one-tailed). That is, the CE signal was stronger than expected by chance for a longer period of time than expected by chance. Observed CE values greater than the bootstrap distribution is same-preferring ($S > D$) and lesser than the bootstrap distribution is different-preferring ($D > S$).

For comparing the magnitude of CE over time for neurons significantly CE-signalling (Figure 2.5), we averaged the CE values over two time windows of interest: the S2 period (0 to 500 ms relative to S2 onset) and the post-S2 period (500 ms to 1.5 s relative to S2 onset). We then tested for the difference in CE between tasks for each group of neurons

(enhanced, suppressed, consistent) for each type of comparison signal ($S > D$, $D > S$) and for each time window of interest using a Kolmogorov-Smirnov with $p < 0.05$ (Bonferroni-corrected for the twelve repeated tests) considered significant.

Chapter 3

Stimulus Optimization for Neural Populations

3.1 Optimization

Consider here, **EXAMPLE OF EASILY-UNDERSTANDIBLE OPTIMIZATION PROBLEM**. This example demonstrates that optimization, at the outset, is a simple problem. The complexity comes from large, high-dimensional data sets, and the plethora of approaches available. In this chapter, I will first describe the two main classes of optimization. Second, I will link these concepts to functional properties of neurons, focusing heavily on the visual system. I will then compare multiple algorithms when optimizing simulated neural data.

What is Optimization?

In its simplest form, optimization begins with an unknown function of inputs $\vec{x}$:

$$f(\vec{x}) : \mathbb{R}^n \rightarrow \mathbb{R} \tag{3.1}$$

where the output of the function is deterministic of it's inputs $\vec{x}$. The goal of optimization is to then find the set of inputs which minimizes (or maximizes) the output of the function $f(\vec{x})$. **MORE INTRO TO THIS SECTION BEFORE DERIVATIVES**

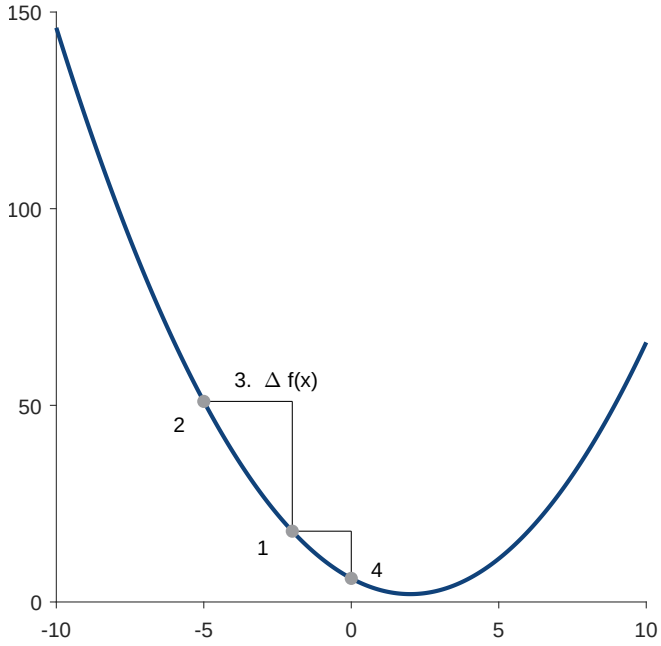

FIGURE 3.1: *FigureTitle*

3.1.1 Derivative-Based Optimization

MORE INTRO TO THIS SUBSECTION We an illustrate this using the simple example of a parabola. In the realm of low-noise and few variables, optimization is a rather simple problem of calculating the gradient and following it (Figure 3.1). In Figure 3.1, we test the function by using two random inputs (points 1&2), calculate the gradient (3), and follow the gradient for the next input (4). This is an iterative process whereby each time we sample the function, we obtain more knowledge about it. Continuing this process will eventually result in $x = 2$ as the global minimum. While this may appear obvious, in real world problems the blue line is unknown, necessitating the use of optimization techniques. Unfortunately, because data is often high-noise and high-dimensional (in the parabola example there is only one input x, but most problems have many), calculating gradients quickly becomes computationally intractable in finite time. In addition to these constraints, real-world problems are often non-convex, meaning they have many local minima where gradient descent fails (**MAYBE NON-CONVEX FIGURE EXAMPLE**). This problem belies standard gradient approaches and lead to the development of Derivative-Free optimization techniques (see 3.1.2).

3.1.2 Derivative-Free Optimization

3.1.3 Manifold Approximation with Particle Swarm (MAPS)

3.1.4 Genetic Algorithm

genetic algorithm doesn't explore the radial dimension well. Even with a-priori knowledge of the proper radius, it doesn't do any better than MAPS because of this (prove it?).

3.1.5 Bayesian estimation of true gradients?

3.1.6 Comparison across algorithms

3.2 Simulated Neural Population

Assumptions:

1. Peak FR= $100\frac{spk}{s}$
2. Independent tuning to each feature dimension
3. Deterministic responses (could fix)
4. Independent Neurons
5. Ground truth stimulus

$x - pref$ is a matrix of euclidean distances for the current stimulus to each individual neurons' preferred stimulus. tuning is the neurons covariance matrix for the latent space (nLatents x nLatents). Diagonal is tuning width in that dimension and 0s off diagonal because feature tuning is assumed independent

$$someSymbol = -(x - pref)^T * tuning * (x - pref) \tag{3.2}$$

response function: (come up with symbols for terms)

$$\vec{y} = Peak * \exp \tag{3.3}$$

Chapter 4

Neural Manafold Approximation with Particle Swarm (nMAPS)

4.1 Introduction

In the previous section I discussed how optimization approaches can circumvent some of the experimental limitations for measuring high-dimensional feature tuning. This was done on model neural populations with a known ground truth. In this section I will discuss similar methodology using electrophysiology recordings in awake and behaving Rhesus Macaques.

Research into sensory coding in the visual system focuses on determining what visual features neuronal activity covaries with, i.e. what information are they encoding. Traditional experiments looked at neural responses to simple stimuli such as small patches of light or oriented bars Hubel and Wiesel, 1959. These stimuli are effective at driving neurons in early visual areas, but produce Weak responses from higher visual areas where neurons prefer complex combinations of many features like contrast, color, orientation, curvature, etc Sani et al., 2013; Tanigawa, Lu, and Roe, 2010; Nandy et al., 2016. In these higher visual areas, like V4, it is not feasible to systematically test every combination of visual features to search for feature tuning. Here I describe a method for efficiently exploring these spaces to find relationships between sensory features and neural responses.

4.2 Methods

4.2.1 Research subject

One adult male rhesus macaque (*Macaca mulatta*) was used for this study. All experimental procedures were approved by the University Committee on Animal Resources at the University of Rochester and performed in accordance with the National Institutes of Health *Guide for the Care and Use of Laboratory Animals* National Research Council, 2011.

4.2.2 Generative Adversarial Networks

Generative adversarial networks (GANs) are a type of artificial neural network that learn low-dimensional representations of higher-dimensional data, such as images Karras, Laine, and Aila, 2019. GANs trained to generate images learned to map high-order image statistics onto a set of 'latent' variables. GANs provide a continuous stimulus space that is constrained to be within a set of plausibly natural images. The images generated by a GAN are more naturalistic than simple Gabors, while also being more tractable to use experimentally than natural images, making them promising tools for vision research. The GAN used in these experiments had a 128-dimensional input (latent) space, and was trained on the Cifar-10 image data set as described previously Fruend and Stalker, 2018.

4.2.3 Particle Swarm

Particle swarm utilizes a hive-mind approach to solve optimization problems. Each 'particle' corresponds to a point in the high dimensional stimulus space (an image), and travels through the space in order to maximize the L^2 norm of the population response. By moving through the stimulus space, the images change along latent feature dimensions, resulting in smooth image manipulation. Particles move through the stimulus space by integrating information about local gradients and neural responses to other

particles. Particles therefore both compete and collaborate in order to explore the stimulus and response spaces.

Manafold Approximation with Particle Swarm (MAPS) is initialized with three generations of random points for each of 64 particles. This gives the kernel regression a history to estimate gradients. For subsequent generations, each particle takes a step S_p according to three terms: the estimated local gradient ∇e_p, the weighted sum of vectors towards particles that resulted in better neural responses G_p, and a momentum term M_p (Equation 1).

$$S_p = c_1 r_{1p} \nabla e_p + c_2 r_{2p} G_p + b M_p \tag{4.1}$$

The constants c_1 and c_2 are learning rates for the gradient and global information components respectively, while $b \in [0, 1]$ is a decay term for the momentum. The stochastic scaling factors r_{1p} and $r_{2p} \sim U(0, 1)$ help circumvent the problem of choosing a correct step size. Too large and particles will jump over maxima, but too small and it will take too long to converge, so step sizes are pulled from a uniform distribution for each particle each generation.

We used kernel regression to estimate the gradient according to each particles' personal history. This way, each particle travels along its' local gradient, independent of how each other particle moves.

$$\nabla e_p(x^*) = \frac{1}{t-1} \sum_{k=1}^{t-1} \nabla w_k(x^*) A_k \tag{4.2}$$

$$\nabla w_k(x^*) = \frac{2K(x^*, x_k) \sum_{l=1}^{t-1} (x_k - x_l) K(x^*, x_l)}{h^2 \left(\sum_{l=1}^{t-1} K(x^*, x_l) \right)^2} \tag{4.3}$$

where

$$A_k = \sum_{j=1}^{t-1} ||r_k|| + ||r_k - r_j|| \tag{4.4}$$

and

$$K(x,y) = e^{-\frac{||x-y||}{h^2}} \tag{4.5}$$

The next component (Equation 4.6) is a weighted sum that uses information about the global response manifold to predict where good parts of the space is. Stimuli that resulted in a large neural response from many neurons pull the particle density toward them. Again, x_p and r_p represent the stimulus embedding vector and the neural response vector respectively for particle p. G_p is the sum of unit vectors towards all the points which resulted in better neural responses $x_k, k = 1, ..., u$, weighted by how much better that response $r_k, k = 1, ..., u$ was than the current point r_p.

$$G_p = \sum_{k=1}^{u} \frac{(||r_k|| - ||r_p||)}{\sum_{j=1}^{u} ||r_j|| - ||r_p||} \frac{x_k - x_p}{||x_k - x_p||} \tag{4.6}$$

4.2.4 Genetic Algorithm

4.2.5 Electrical Recordings

Prior to any electrical recordings, the subject was first implanted with a titanium head holder, trained on behavioral tasks, and then implanted with chronic electrode arrays. All surgeries we performed with isoflurane anesthesia, aseptic technique, and perioperative opiate analgesics.

Head Holder Implantation. The subject was initially sedated with a 10mg/kg intramuscular injection of ketamine and administered with 0.25mg/kg midazolam, 0.011mg/kg glycopyrrolate, 25mg/kg cefazolin, and 0.2mg/kg meloxicam, all intramuscular. Once anesthetized, we intubated the animal with an endotrachial tube, shaved the animals head, inserted a catheter in the small saphenous vein for infusion of lactated Ringer's solution, then positioned the head in a stereotaxic frame. The anesthesia was maintained with 1.5% isoflourane throughout the surgery. The surgical site was then thoroughly scrubbed with povidone iodine solution in the preparation of the sterile field. We made a horseshoe-shaped incision (6cm wide by 10cm anterior-posterior) using a #10 scalpel blade starting from the right brow, cutting caudally parallel to the midline, and ending

at the left brow. We then used bone curettes to retract the tissue and clear a large enough surface of skull for the head holder. Sterile gauze soaked in saline was used to keep the tissue moist throughout the surgery. The prefabricated titanium head holder (custum design machined by the university of Pittsburgh cite mat?) attaches to the skull using 16 6mm titanium screws (Veterinary Orthopedic Implants, Saint Augustine, FL) that go through 6 flange straps radially extending from the center of its base. We next bent the straps of the head holder so it fit tightly on the skull. We marked with pencil the final position of the head holder on the skull and made two small incisions in an x through the retracted tissue where the head holder would protrude. We then pushed the exterior portion of the head holder through the dermostomy in the retracted tissue and repositioned it back on the skull. We used a 2mm surgical drillbit and a custum drill stop set to the thickness of the skull to drill through the skull, starting with the lateral-most location of the head holder. Skrews were implanted one a time, alterniting across the midline, lateral to medial. Once each screw was implanted we used geristore (DenMat, Lompoc, CA, USA) to fill any gaps between the skull and head holder. After the geristor fully dried, we sutured the wound using a continuous running stitch to attach the subcutaneous fascia and simple interrupted stitches on top to fully connect the skin around the wound margin. Intramuscular injections of 25mg/kg cefazolin were administered every 12h for seven days post op, and 0.2mg/kg meloxicam every 24h for 3 days post op. The subject was allowed one month to recover before the start of training.

Behavioral Training. Prior to array implantation, the animal first underwent fixation training. The monkey sits 50cm away from a 120Hz ViewPixx/3D monitor (VPixx Technologies, Saint-Bruno, QC, Canada). We used Matlab (The MathWorks, Inc) and Psychtoolbox to control the experiments and present visual stimuli. Eye position was tracked with an Eyelink 1000 IR eye tracking camera (SR Research, Ottawa, Ontario, Canada), and the monkey was given water reward for fixating on a central dot. Once the monkey understood the basic reward contingencies he was implanted with two 128 channel matrix electrode arrays (NeuroNexus, Ann Arbor, MI, USA).

Array Implantation. The monkey was given intramuscular injections of ketamine,

medazolam, glycopyrrolate, cefazolin, and meloxicam at the same doses described earlier for the headpost holder surgery. Similarly, the monkey was intubated, shaved, catheterized, and positioned in the stereotactic frame in the same manner. Again the animal was maintained on 1.5% anesthesia throughout the surgery. We marked the stereotactic coordinates for prefrontal cortex (30mm anterior, 21mm lateral, 25mm dorsal) and visual area V4 (0mm anterior, 0mm lateral, 27mm dorsal) as well as estimated locations for the two array pedestals (NeuroNexus, Ann Arbor, MI, USA) prior to making the incision. Once we planned out the location of the pedestals and craniotomies we made the incision with a size 10 scalpel blade, starting on the posterior surface of the cranium. The incision was made just off the midline (away from the hemisphere we implanted in) and continued until about 1cm away from the margin around the head holder, leaving room to ensure that enough healthy tissue remained between the incision and head holder. We then cut a hemicircle around the head holder, again leaving enough healthy tissue to be able to suture the wound and continued just off the midline up to the brow. The final incision started halfway through the hemicircular incision, perpendicular to the midline, and continued 10cm laterally. We used bone curettes to retract the tissue while minimizing muscle damage, and again kept the retracted tissue hydrated with sterile gauze and saline. Once the skull was sufficiently cleaned, we marked the location of the craniotomies in pencil using stereotactic coordinates. The pedestals were both placed on the midline, one anterior to the head holder (PFC), and the other posterior to the head holder (V4). Similar to the head holder surgery, we then bent the legs of the two pedestals to fit tightly onto the skull and marked the location of each screw with a pencil. The animal was then administered a second intramuscular dose of cefazolin. We used 8 and 10 6mm titanium screws (Veterinary Orthopedic Implants, Saint Augustine, FL) for the PFC and V4 pedestals respectively. After the pedestals were secured we used a 19mm diameter trephine to do the PFC craniotomy followed by kerrison punches to remove any pieces of bone around the perimeter. The animal was then administered a 0.5mg/kg intramuscular dose of dexmethasone. Afterward, we used a drimmel to smooth down a trench going from the pedestal to the

craniotomy in order to prevent the wire bundle from snagging or bending. We next cut the dura on three sides of a 1cm square and retracted it. A 128 channel matrix electrode array (NeuroNexus, Ann Arbor, MI, USA) was inserted dorsal to the principal sulcus, using a microdriver (Zaber, Vancouver, British Columbia, Canada) attached to an all-angle manipulator (NeuroNexus, Ann Arbor, MI, USA). Once the array was in place, we inserted the reference wire under the dura, sutured it closed with nurolon sutures (5-0 dissolving sutures), and covered the craniotomy with duragen (Integra Life Sciences co.). The animal was injected with Buprinex SR IM every two hours, starting 6 hours into the surgery until we finished. We then used two titanium plates to cover and protect the craniotomy by screwing them into the skull in the same manner as the pedestals and headpost. After the craniotomy was secure we covered the trench and wire bundle with kwik-sil and filled any gaps under the PFC pedestal with geristore. We then sutured around the anterior wound margin back to the lateral incision using the same procedure as the head holder sutures. These same steps from craniotomy to suturing were replicated for the implantation of the V4 array. Post operative care included administration of 25mg/kg cefazolin every 12h for seven days, and 0.2mg/kg meloxicam every 24h for 3 days.

4.2.6 Data Analysis

All data was analyzed with Matlab 2018b (The MathWorks, Inc) statistics and machine learning toolbox. A neuron's response was defined as the number of threshold crossings (-4 standard deviations below the median noise) that occurred in a 200ms window from stimulus onset. Channels with unrealistic firing rates above 300 Hz (ie. 60+ spikes within the window) had their responses set to 0 so as to not adversely affect the optimization algorithm. Additionally, if the population response on any trial resulted in too large an L^2 norm, this was assumed to be due to noise and the trial was repeated before the end of the block. We used canonical correlations analysis (CCA) and distance covariance analysis (DCA) to analyze relative linear and nonlinear relationships

between the GAN latent space and neural response space Cowley et al., 2017b.

4.3 High-Dimensional Feature Tuning

4.3.1 Neurons multiplex

4.3.2 How they multiplex is a mystery in V4

4.3.3 Stimulus encoding is a population-level problem

4.4 High-dimensional feature spaces (GAN)

4.4.1 WTF is a latent variable model

4.4.2 WTF is a GAN? also why would you do this to yourself?

4.5 Comparing two high-dimensional spaces

4.5.1 Population-level results

4.5.2 Individual Neuron results

4.5.3 Converting "latents" back into english

Bibliography

Arandia-Romero, Iñigo et al. (2016). "Multiplicative and Additive Modulation of Neuronal Tuning with Population Activity Affects Encoded Information". In: *Neuron* 89.6, pp. 1305–1316. ISSN: 10974199. DOI: 10.1016/j.neuron.2016.01.044.

Barbas, H. (1988). "Anatomic organization of basoventral and mediodorsal visual recipient prefrontal regions in the rhesus monkey". In: *Journal of Comparative Neurology* 276.3, pp. 313–342. ISSN: 10969861. DOI: 10.1002/cne.902760302.

Barone, Pascal et al. (2000). "Laminar distribution of neurons in extrastriate areas projecting to visual areas V1 and V4 correlates with the hiearchical rank and intimates the operation of a distance rule". In: *Journal of Neuroscience* 20.9, pp. 3263–3281. ISSN: 02706474. DOI: 10.1523/jneurosci.20-09-03263.2000.

Batardiere, A. (2002). "Early Specification of the Hierarchical Organization of Visual Cortical Areas in the Macaque Monkey". In: *Cerebral Cortex* 12.5, pp. 453–465. ISSN: 1047-3211. DOI: 10.1093/cercor/12.5.453.

Bisley, James W. and Tatiana Pasternak (2000). "The multiple roles of visual cortical areas MT/MST in remembering the direction of visual motion". In: *Cerebral Cortex* 10.11, pp. 1053–1065. ISSN: 10473211. DOI: 10.1093/cercor/10.11.1053.

Bisley, James W., Daniel Zaksas, and Tatiana Pasternak (2001). "Microstimulation of cortical area MT affects performance on a visual working memory task". In: *Journal of Neurophysiology* 85.1, pp. 187–196. ISSN: 00223077. DOI: 10.1152/jn.2001.85.1.187.

Bisley, James W. et al. (2004). "Activity of Neurons in Cortical Area MT during A Memory for Motion Task". In: *Journal of Neurophysiology* 91.1, pp. 286–300. ISSN: 00223077. DOI: 10.1152/jn.00870.2003.

Born, Richard T. and David C. Bradley (2005). "Structure and function of visual area MT". In: *Annual Review of Neuroscience* 28, pp. 157–189. ISSN: 0147006X. DOI: 10.1146/annurev.neuro.26.041002.131052.

Bredfeldt, C E and D L Ringach (2002). "Dynamics of Spatial Frequency Tuning in Macaque V1". In: 22.5, pp. 1976–1984.

Britten, K. H. et al. (1992). "The analysis of visual motion: A comparison of neuronal and psychophysical performance". In: *Journal of Neuroscience* 12.12, pp. 4745–4765. ISSN: 02706474. DOI: 10.1523/jneurosci.12-12-04745.1992.

Butts, Daniel A and Mark S Goldman (2006). "Tuning Curves , Neuronal Variability , and Sensory Coding". In: 4.4. DOI: 10.1371/journal.pbio.0040092.

Chung, Sueyeon, Daniel D Lee, and Haim Sompolinsky (2018). "Classification and Geometry of General Perceptual Manifolds". In: *Physical Review X* 8.3, p. 31003. ISSN: 2160-3308. DOI: 10.1103/PhysRevX.8.031003. URL: https://doi.org/10.1103/PhysRevX.8.031003.

Churchland, Mark M. et al. (2010). "Stimulus onset quenches neural variability: A widespread cortical phenomenon". In: *Nature Neuroscience* 13.3, pp. 369–378. ISSN: 10976256. DOI: 10.1038/nn.2501. URL: http://dx.doi.org/10.1038/nn.2501.

Cohen, M. R. and J. H. R. Maunsell (2010). "A Neuronal Population Measure of Attention Predicts Behavioral Performance on Individual Trials". In: *Journal of Neuroscience* 30.45, pp. 15241–15253. ISSN: 0270-6474. DOI: 10.1523/JNEUROSCI.2171-10.2010. URL: http://www.jneurosci.org/cgi/doi/10.1523/JNEUROSCI.2171-10.2010.

Cohen, Marlene R. and William T. Newsome (2008). "Context-Dependent Changes in Functional Circuitry in Visual Area MT". In: *Neuron* 60.1, pp. 162–173. ISSN: 08966273. DOI: 10.1016/j.neuron.2008.08.007.

Cowley, Benjamin et al. (2017a). "Adaptive stimulus selection for optimizing neural population responses". In: *Advances in Neural Information Processing Systems 30* Nips, pp. 1396–1406. ISSN: 10495258. URL: http://papers.nips.cc/paper/6738-adaptive-stimulus-selection-for-optimizing-neural-population-responses.pdf.

Cowley, Benjamin R. et al. (2017b). "Distance covariance analysis". In: *Proceedings of the 20th International Conference on Artificial Intelligence and Statistics, AISTATS 2017*.

Cross, Logan et al. (2021). "Using deep reinforcement learning to reveal how the brain encodes abstract state-space representations in high-dimensional environments". In: *Neuron*, pp. 1–15. ISSN: 10974199. DOI: 10.1016/j.neuron.2020.11.021. URL: https://doi.org/10.1016/j.neuron.2020.11.021.

Denfield, George H. et al. (2018). "Attentional fluctuations induce shared variability in macaque primary visual cortex". In: *Nature Communications* 9.1. ISSN: 20411723. DOI: 10.1038/s41467-018-05123-6.

Ding, Long (2015). "Distinct dynamics of ramping activity in the frontal cortex and caudate nucleus in monkeys". In: *Journal of Neurophysiology* 114.3, pp. 1850–1861. ISSN: 15221598. DOI: 10.1152/jn.00395.2015.

Ecker, Alexander S. et al. (2016). "On the structure of neuronal population activity under fluctuations in attentional state". In: *Journal of Neuroscience* 36.5, pp. 1775–1789. ISSN: 15292401. DOI: 10.1523/JNEUROSCI.2044-15.2016.

Felleman, Daniel J. and David C. Van Essen (1991). "Distributed hierarchical processing in the primate cerebral cortex". In: *Cerebral Cortex* 1.1, pp. 1–47. ISSN: 14602199. DOI: 10.1093/cercor/1.1.1.

Felleman, Daniel J., Youping Xiao, and Evelyn McClendon (1997). "Modular organization of occipito-temporal pathways: Cortical connections between visual area 4 and visual area 2 and posterior inferotemporal ventral area in macaque monkeys". In: *Journal of Neuroscience* 17.9, pp. 3185–3200. ISSN: 02706474. DOI: 10.1523/jneurosci.17-09-03185.1997.

Field, Greg D. et al. (2010). "Functional connectivity in the retina at the resolution of photoreceptors". In: *Nature* 467.7316, pp. 673–677. ISSN: 00280836. DOI: 10.1038/nature09424. URL: http://dx.doi.org/10.1038/nature09424.

Fruend, Ingo and Elee Stalker (2018). "Human sensitivity to perturbations constrained by a model of the natural image manifold". In: *Journal of Vision* 18.11, p. 20. ISSN:

1534-7362. DOI: 10.1167/18.11.20. URL: http://jov.arvojournals.org/article.aspx?doi=10.1167/18.11.20.

Gilbert, Charles D. and Wu Li (2013). "Top-down influences on visual processing". In: *Nature Reviews Neuroscience* 14.5, pp. 350–363. ISSN: 1471003X. DOI: 10.1038/nrn3476.

Hatsopoulos, N. G. et al. (1998). "Information about movement direction obtained from synchronous activity of motor cortical neurons". In: *Proceedings of the National Academy of Sciences of the United States of America* 95.26, pp. 15706–15711. ISSN: 00278424. DOI: 10.1073/pnas.95.26.15706.

Hubel, David and T Wiesel (1959). "Receptive Fields of Single Neurones in the Cat's Striate Cortex". In: *J. Physiol.* Pp. 574–591.

Hubel, David H. and Torsten N. Wiesel (1965). "Receptive Fields and Functional Architecture in Two Nonstriate Visual Areas (18 and 19) of the Cat". In: *Journal of Neurophysiology* 28.2, pp. 229–289. ISSN: 0022-3077. DOI: 10.1152/jn.1965.28.2.229. URL: http://www.physiology.org/doi/10.1152/jn.1965.28.2.229.

Hussar, Cory and Tatiana Pasternak (2010). "Trial-to-trial variability of the prefrontal neurons reveals the nature of their engagement in a motion discrimination task". In: *Proceedings of the National Academy of Sciences of the United States of America* 107.50, pp. 21842–21847. ISSN: 00278424. DOI: 10.1073/pnas.1009956107.

Hussar, Cory R. and Tatiana Pasternak (2009). "Flexibility of Sensory Representations in Prefrontal Cortex Depends on Cell Type". In: *Neuron* 64.5, pp. 730–743. ISSN: 08966273. DOI: 10.1016/j.neuron.2009.11.018. URL: http://dx.doi.org/10.1016/j.neuron.2009.11.018.

— (2012). "Memory-guided sensory comparisons in the prefrontal cortex: Contribution of putative pyramidal cells and interneurons". In: *Journal of Neuroscience* 32.8, pp. 2747–2761. ISSN: 02706474. DOI: 10.1523/JNEUROSCI.5135-11.2012.

— (2013). "Common rules guide comparisons of speed and direction of motion in the dorsolateral prefrontal cortex". In: *Journal of Neuroscience* 33.3, pp. 972–986. ISSN: 02706474. DOI: 10.1523/JNEUROSCI.4075-12.2013.

Karras, Tero, Samuli Laine, and Timo Aila (2019). "A style-based generator architecture for generative adversarial networks". In: *Proceedings of the IEEE Computer Society Conference on Computer Vision and Pattern Recognition* 2019-June, pp. 4396–4405. ISSN: 10636919. DOI: 10.1109/CVPR.2019.00453. arXiv: 1812.04948.

Katz, Leor N. et al. (2016). "Dissociated functional significance of decision-related activity in the primate dorsal stream". In: *Nature* 535.7611, pp. 285–288. ISSN: 14764687. DOI: 10.1038/nature18617.

Kohn, Adam and J. Anthony Movshon (2003). "Neuronal adaptation to visual motion in area MT of the macaque". In: *Neuron* 39.4, pp. 681–691. ISSN: 08966273. DOI: 10.1016/S0896-6273(03)00438-0.

Kriegeskorte, Nikolaus and Xue Xin Wei (2021). "Neural tuning and representational geometry". In: *Nature Reviews Neuroscience*. ISSN: 14710048. DOI: 10.1038/s41583-021-00502-3. arXiv: 2104.09743.

Lennie, P., J. Krauskopf, and G. Sclar (1990). "Chromatic mechanisms in striate cortex of macaque". In: *Journal of Neuroscience* 10.2, pp. 649–669. ISSN: 02706474. DOI: 10.1523/jneurosci.10-02-00649.1990.

Liu, Ye et al. (2020). "Hierarchical Representation for Chromatic Processing across Macaque V1, V2, and V4". In: *Neuron* 108.3, 538–550.e5. ISSN: 10974199. DOI: 10.1016/j.neuron.2020.07.037.

Luck, Steven J. et al. (1997). "Neural mechanisms of spatial selective attention in areas V1, V2, and V4 of macaque visual cortex". In: *Journal of Neurophysiology* 77.1, pp. 24–42. ISSN: 00223077. DOI: 10.1152/jn.1997.77.1.24. URL: http://www.physiology.org/doi/10.1152/jn.1997.77.1.24.

Lui, Leo L. and Tatiana Pasternak (2011). "Representation of comparison signals in cortical area MT during a delayed direction discrimination task". In: *Journal of Neurophysiology* 106.3, pp. 1260–1273. ISSN: 00223077. DOI: 10.1152/jn.00016.2011.

Mahon, L E and R L D E Valois (2001). "Cartesian and non-Cartesian responses in LGN , V1 , and V2 cells". In: 2001, pp. 973–981.

Martinez-Trujillo, Julio and Stefan Treue (2004). "Feature-Based Attention Increases the Selectivity of Population Responses in Primate Visual Cortex". In: *Current Biology* 14, p. 1118. DOI: 10.1016/j.

Mitchell, Jude F., Kristy A. Sundberg, and John H. Reynolds (2007). "Differential Attention-Dependent Response Modulation across Cell Classes in Macaque Visual Area V4". In: *Neuron* 55.1, pp. 131–141. ISSN: 08966273. DOI: 10.1016/j.neuron.2007.06.018.

Moreno-Bote, Rubén et al. (2014). "Information-limiting correlations". In: *Nature Neuroscience* 17.10, pp. 1410–1417. ISSN: 15461726. DOI: 10.1038/nn.3807.

Nandy, Anirvan S et al. (2016). "Neurons in Macaque Area V4 Are Tuned for Complex Spatio-Temporal Patterns". In: *Neuron* 91.4, pp. 920–930. ISSN: 0896-6273. DOI: 10.1016/j.neuron.2016.07.026. URL: http://dx.doi.org/10.1016/j.neuron.2016.07.026.

Narayanan, Nandakumar S. (2016). "Ramping activity is a cortical mechanism of temporal control of action". In: *Current Opinion in Behavioral Sciences* 8, pp. 226–230. ISSN: 23521546. DOI: 10.1016/j.cobeha.2016.02.017.

National Research Council (2011). *Guide for the Care and Use of Laboratory Animals*. 8th Editio. ISBN: 9780309154000.

Paninski, Liam et al. (2010). "A new look at state-space models for neural data". In: *Journal of Computational Neuroscience* 29.1-2, pp. 107–126. ISSN: 09295313. DOI: 10.1007/s10827-009-0179-x.

Pasternak, Tatiana and Duje Tadin (2020). "Linking Neuronal Direction Selectivity to Perceptual Decisions about Visual Motion". In: *Annual Review of Vision Science* 6, pp. 335–362. ISSN: 23744650. DOI: 10.1146/annurev-vision-121219-081816.

Pasupathy, Anitha and Charles E. Connor (2002). "Population coding of shape in area V4". In: *Nature Neuroscience* 5.12, pp. 1332–1338. ISSN: 10976256. DOI: 10.1038/nn972.

Petrides, M. and D. N. Pandya (2006). "Efferent Association Pathways Originating in the Caudal Prefrontal Cortex in the Macaque Monkey". In: *Journal of Comparative Neurology* 498.October 2007, pp. 227–251. DOI: 10.1002/cne.

Ponce, Carlos R. et al. (2019). "Evolving Images for Visual Neurons Using a Deep Generative Network Reveals Coding Principles and Neuronal Preferences". In: *Cell* 177.4, 999–1009.e10. ISSN: 10974172. DOI: 10.1016/j.cell.2019.04.005. URL: http://dx.doi.org/10.1016/j.cell.2019.04.005.

Ponce-Alvarez, Adrián et al. (2013). "Stimulus-dependent variability and noise correlations in cortical MT neurons". In: *Proceedings of the National Academy of Sciences of the United States of America* 110.32, pp. 13162–13167. ISSN: 00278424. DOI: 10.1073/pnas.1300098110.

Quian Quiroga, Rodrigo and Stefano Panzeri (2009). "Extracting information from neuronal populations: Information theory and decoding approaches". In: *Nature Reviews Neuroscience* 10.3, pp. 173–185. ISSN: 1471003X. DOI: 10.1038/nrn2578.

Rajdl, K., P. Lansky, and L. Kostal (2017). "Entropy factor for randomness quantification in neuronal data". In: *Neural Networks* 95, pp. 57–65. ISSN: 18792782. DOI: 10.1016/j.neunet.2017.07.016.

Renart, Alfonso and Christian K. Machens (2014). "Variability in neural activity and behavior". In: *Current Opinion in Neurobiology* 25, pp. 211–220. ISSN: 18736882. DOI: 10.1016/j.conb.2014.02.013.

Rudolph, Kirsten and Tatiana Pasternak (1999). "Transient and permanent deficits in motion perception after lesions of cortical areas MT and MST in the macaque monkey". In: *Cerebral Cortex* 9.1, pp. 90–100. ISSN: 10473211. DOI: 10.1093/cercor/9.1.90.

Ruff, Douglas A and Marlene R Cohen (2016). "Attention Increases Spike Count Correlations between Visual Cortical Areas". In: 36.28, pp. 7523–7534. DOI: 10.1523/JNEUROSCI.0610-16.2016.

Salzman, C. D. et al. (1992). "Microstimulation in visual area MT: Effects on direction discrimination performance". In: *Journal of Neuroscience* 12.6, pp. 2331–2355. ISSN: 02706474. DOI: 10.1523/jneurosci.12-06-02331.1992.

Salzman, C. Daniel, Kenneth H. Britten, and William T. Newsome (1990). "Cortical microstimulation influences perceptual judgements of motion direction". In: *Nature* 346.6280, pp. 174–177. ISSN: 00280836. DOI: 10.1038/346174a0.

Sani, Ilaria et al. (2013). "Selective Tuning for Contrast in Macaque Area V4". In: 33.47, pp. 18583–18596. DOI: 10.1523/JNEUROSCI.3465-13.2013.

Seriès, Peggy, Peter E. Latham, and Alexandre Pouget (2004). "Tuning curve sharpening for orientation selectivity: Coding efficiency and the impact of correlations". In: *Nature Neuroscience* 7.10, pp. 1129–1135. ISSN: 10976256. DOI: 10.1038/nn1321.

Shadlen, Michael N. and William T. Newsome (2001). "Neural Basis of a Perceptual Decision in the Parietal Cortex (Area LIP) of the Rhesus Monkey". In: *Journal of Neurophysiology* 86.4, pp. 1916–1936. ISSN: 0022-3077. DOI: 10.1152/jn.2001.86.4.1916. URL: http://www.physiology.org/doi/10.1152/jn.2001.86.4.1916.

Snyder, A.C. et al. (2014). "Correlations in V1 are reduced by stimulation outside the receptive field". In: *Journal of Neuroscience* 34.34. ISSN: 15292401. DOI: 10.1523/JNEUROSCI.0762-14.2014.

Snyder, Adam C., Byron M. Yu, and Matthew A. Smith (2018). "Distinct population codes for attention in the absence and presence of visual stimulation". In: *Nature Communications* 9.1. ISSN: 20411723. DOI: 10.1038/s41467-018-06754-5.

— (2021). "A Stable Population Code for Attention in Prefrontal Cortex Leads a Dynamic Attention Code in Visual Cortex". In: *The Journal of Neuroscience* 41.44, pp. 9163–9176. ISSN: 0270-6474. DOI: 10.1523/jneurosci.0608-21.2021.

Tanigawa, Hisashi, Haidong D. Lu, and Anna W. Roe (2010). "Functional organization for color and orientation in macaque V4". In: *Nature Neuroscience* 13.12, pp. 1542–1549. ISSN: 10976256. DOI: 10.1038/nn.2676.

Ungerleider, Leslie G. and Robert Desimone (1986). "Cortical connections of visual area MT in the macaque". In: *Journal of Comparative Neurology* 248.2, pp. 190–222. ISSN: 10969861. DOI: 10.1002/cne.902480204.

Wiesel, Torsten N. (1959). "Recording Inhibition and Excitation in the Cat's Retinal Ganglion Cells with intracellular Electrodes". In: *Nature* 1, pp. 21–22.

Wimmer, K. et al. (2016). "Transitions between Multiband Oscillatory Patterns Characterize Memory-Guided Perceptual Decisions in Prefrontal Circuits". In: *Journal of Neuroscience* 36.2, pp. 489–505. ISSN: 0270-6474. DOI: 10.1523/JNEUROSCI.3678-15.2016. URL: http://www.jneurosci.org/cgi/doi/10.1523/JNEUROSCI.3678-15.2016.

Yoshioka, Takashi, Bruce M. Dow, and Robert G. Vautin (1996). "Neuronal mechanisms of color categorization in areas V1, V2 and V4 of macaque monkey visual cortex". In: *Behavioural Brain Research* 76.1-2, pp. 51–70. ISSN: 01664328. DOI: 10.1016/0166-4328(95)00183-2.

Zaksas, Daniel and Tatiana Pasternak (2006). "Directional signals in the prefrontal cortex and in area MT during a working memory for visual motion task". In: *Journal of Neuroscience* 26.45, pp. 11726–11742. ISSN: 02706474. DOI: 10.1523/JNEUROSCI.3420-06.2006.